

---

---

# Analysis of aerodynamic stability of long-span suspended bridges

---

---



Author: **Carlos Cordeiro**

Supervisor: **Søren R.K. Nielsen**

**Department of Civil Engineering**

AALBORG UNIVERSITY

This dissertation is submitted for the degree of  
*MSc. in Structural and Civil Engineering*  
September 2017 – June 2018



This thesis is dedicated to those, family, friends and teachers who always believed in my capabilities to pursue my dreams, and in a very special and particular way, dedicated to my life partner, Dorota, for the unconditional support and understanding for the long hours which I dedicated to this work in impairment to the family time.



## **ACKNOWLEDGEMENTS**

I would like to express my gratitude and appreciation to the thesis supervisor, Professor Søren Rasmus Kærshøj Nielsen, for all the dedication and willingness to help and support along all the thesis period. His extensive knowledge and enthusiasm in sharing it was a crucial factor without which this thesis would never have been possible.

Along the way, several persons have had an important role helping out solving relevant and persistent issues. A special thanks goes to Professor Torben Brøchner (VIA University College), Dr.-Ing. Nazim Nariman (Bauhaus University Weimar) and Dr.-Ing. Nils Wagner (INTES GmbH) for all the valuable inputs regarding the structural dynamic numerical model.

I would like to thank COWI, on the person of Allan Larsen, and Sund og Bælt, on the person of Martin Duus Hansen, for providing the needed drawings and data of the Great Belt Bridge.

Finally, I would like to thank to Tony Lindkold from AirFlix.dk for the allowance given to use the picture on the cover page of this thesis.



## ABSTRACT

On 26<sup>th</sup> July 1820, the one which is considered as the first suspended bridge was opened ([11]). Union Chain Bridge, spans only 137m connecting England to Scotland. Almost 100 years later, on 25<sup>th</sup> October 1931, George Washington Bridge, in New York, surpass the milestone of 1000m suspended span ([4]).

From that time ahead, the challenges are increasing exponentially, and the goal of reaching suspended spans of two or three thousand meters is now a reality. At the same time, designers are asked to keep the structures lightweight, slender and flexible but, at the same time, large enough to carry the future traffic demands.

The combination of all these factors made the engineering science to look into details such as aerodynamics. The effect of wind on suspended bridges, and in any structure in general, can result in catastrophic events as happened on 7<sup>th</sup> November 1940 with Tacoma Narrows Bridge ([10]).

The passion about bridges, and in particular, the challenges presented by the aerodynamic analysis, were the motivational core of the author. The reader will be presented with an aerodynamic analysis of three systems based on up-scaled models of a referential bridge (Great Belt Bridge, Denmark). The aim of the present thesis is to describe and evaluate the procedure for investigate the onset of flutter for long-span systems, through a new theory which differs from Scanlan [9]. The entire procedure is developed since the definition of the cable geometry and its stiffness onto the evaluation of aerodynamic parameters.

Due to the complexity of the topic, the author assumes that the reader possesses significant knowledge regarding structural dynamics and aeroelasticity.



# TABLE OF CONTENTS

<b>List of figures</b>	<b>xi</b>
<b>List of tables</b>	<b>xiii</b>
<b>Nomenclature</b>	<b>xv</b>
<b>1 Introduction</b>	<b>1</b>
1.1 Problem formulation . . . . .	1
1.2 Methodology . . . . .	2
1.3 Thesis content . . . . .	2
1.4 Reference bridge and up-scaled models . . . . .	3
1.5 Scaling assumptions . . . . .	4
<b>2 Cable geometry</b>	<b>7</b>
2.1 Cable elements formulation . . . . .	7
2.1.1 Main span . . . . .	7
2.1.2 Side span . . . . .	11
2.2 Results . . . . .	13
<b>3 Structural Dynamics</b>	<b>15</b>
3.1 Description of the model . . . . .	15
3.2 Material properties . . . . .	16
3.2.1 Cable system . . . . .	16
3.2.2 Hangers . . . . .	17
3.2.3 Pylons . . . . .	17
3.2.4 Bridge girder . . . . .	18
3.3 Model validation . . . . .	19
3.4 Outputs from dynamic analysis . . . . .	20

<b>4</b>	<b>Aerodynamics</b>	<b>25</b>
4.1	Modal analysis . . . . .	25
4.2	Frequency response analysis . . . . .	27
4.3	Flutter . . . . .	29
4.4	Reduction of system of equations . . . . .	30
<b>5</b>	<b>Evaluation of aerodynamic parameters</b>	<b>33</b>
5.1	Background in CFD . . . . .	33
5.2	Description of the CFD model . . . . .	34
5.2.1	Inputs . . . . .	34
5.2.2	Domain size . . . . .	35
5.2.3	Mesh size . . . . .	36
5.2.4	Physics and solver . . . . .	38
5.3	Response functions . . . . .	39
5.4	Evaluation of $\Omega_c$ and $V_c$ . . . . .	43
5.5	Dependency of the frequency response function on $\omega$ and $V$ . . . . .	44
<b>6</b>	<b>Conclusion</b>	<b>49</b>
	<b>Bibliography</b>	<b>51</b>
	<b>Appendix A Project drawings from Storebælt Bridge</b>	<b>53</b>
	<b>Appendix B Cross sectional parameters of girder</b>	<b>59</b>

## LIST OF FIGURES

1.1	Up-scaling of pylons . . . . .	6
2.1	Main span statical model . . . . .	8
2.2	Flowchart of the algorithm for main span . . . . .	10
2.3	Side span statical model . . . . .	11
2.4	Flowchart of the algorithm for side span . . . . .	12
2.5	Equilibrium suspension of cables in main span . . . . .	13
2.6	Equilibrium suspension of cables in side span . . . . .	14
3.1	Coordinate system and model orientation . . . . .	16
3.2	Notation for section properties of pylons . . . . .	18
3.3	First symmetric bending mode $j = 1$ (referential bridge) . . . . .	21
3.4	Second symmetric bending mode $j = 3$ (referential bridge) . . . . .	21
3.5	Third symmetric bending mode $j = 7$ (referential bridge) . . . . .	22
3.6	First symmetric torsional mode $j = 5$ (referential bridge) . . . . .	22
4.1	Notation . . . . .	25
5.1	Frequency response function for $p(t)$ due to harmonic varying displacement and velocity of the bridge deck . . . . .	34
5.2	Main domain size . . . . .	36
5.3	Mesh domains and refinements . . . . .	37
5.4	Time series for the normalized and centralized load per unit length due to a harmonic varying vertical velocity of the bridge deck . . . . .	39
5.5	Time series for the normalized and centralized moment load per unit length due to a harmonic varying velocity displacement of the bridge deck . . . . .	40
5.6	Time series for the normalized and centralized load per unit length due to a harmonic varying angular velocity of the bridge deck . . . . .	40

5.7	Time series for the normalized and centralized moment load per unit length due to a harmonic varying angular velocity of the bridge deck . . . . .	41
5.8	Variation of $\Pi_{\dot{u}}(t)$ ; Red curve, $\omega = 0.8 \frac{\text{rad}}{\text{s}}$ , Blue curve, $\omega = 0.4 \frac{\text{rad}}{\text{s}}$ . . . . .	45
5.9	Variation of $\Lambda_{\dot{u}}(t)$ ; Red curve, $\omega = 0.8 \frac{\text{rad}}{\text{s}}$ , Blue curve, $\omega = 0.4 \frac{\text{rad}}{\text{s}}$ . . . . .	45
5.10	Variation of $\Pi_{\dot{\theta}}(t)$ ; Red curve, $\omega = 0.8 \frac{\text{rad}}{\text{s}}$ , Blue curve, $\omega = 0.4 \frac{\text{rad}}{\text{s}}$ . . . . .	46
5.11	Variation of $\Lambda_{\dot{\theta}}(t)$ ; Red curve, $\omega = 0.8 \frac{\text{rad}}{\text{s}}$ , Blue curve, $\omega = 0.4 \frac{\text{rad}}{\text{s}}$ . . . . .	46

## LIST OF TABLES

1.1	Up-scaled values for cross section area of cables . . . . .	4
1.2	Up-scaled values for side span length . . . . .	5
3.1	Material properties . . . . .	17
3.2	Sectional properties of the pylons (referential bridge) . . . . .	17
3.3	Section properties for bridge girder . . . . .	18
3.4	Reference values from modal analysis . . . . .	19
3.5	Eigenfrequencies for referential and up-scaled bridges . . . . .	20
3.6	Non-dimensional quantities $a_{jk}$ . . . . .	23
5.1	Mesh input parameters . . . . .	38
5.2	Phase lag $\phi$ . . . . .	42
5.3	Frequency response functions and phase lags . . . . .	47



# NOMENCLATURE

## Acronyms

CFD	Computational Fluid Dynamics
DOF	Degree-of-freedom
FEM	Finite Elements Method

## Greek letters

$\Lambda_i$	Non-dimensional frequency response quantities due to harmonic varying rotation ( $i = u, \theta$ )
$\mu$	Mass per unit length of bridge girder plus cables
$\mu_c, \mu_{c,0}$	Mass per unit length of suspension cable, on referential bridge
$\mu_b$	Mass per unit length of bridge girder
$\omega$	Undamped angular eigenfrequency
$\Omega, \Omega_c$	Non-dimensional reduced angular frequency, critical value
$\phi$	Phase lag
$\Pi_i$	Non-dimensional frequency response quantities due to harmonic varying vertical displacement ( $i = u, \theta$ )
$\Phi$	Undamped eigenmode vector
$\rho_c, \rho_h$	Material density of cables; hangers
$\sigma_0$	Allowable stress
$\theta, \Theta$	Rotation in $z$ -direction, Normalized rotation vector in $z$ -direction
$\zeta$	Structural modal damping ratio

## Notation

$\mathbf{A}_a$	Amplitude vector
$\mathbf{H}_a$	Frequency response matrix
$\mathbf{U}$	Complex amplitude vector
$A_b, A_c, A_h$	Cross sectional area of bridge girder, cable, hanger

$dS$	Spatial discretization along cable length
$dx, dy$	Spatial discretization along $x$ -axis, along $y$ -axis
$f, f_j, \mathbf{f}$	Undamped eigenfrequency; Modal load of $j$ th mode; Modal load vector
$f_j$	Undamped eigenfrequency of the $j$ th mode
$g$	Gravitational acceleration
$H, H_0$	Horizontal force on cables, Horizontal force on cables of referential bridge
$h_0$	Cable camber of referential bridge
$h_p$	Critical buckling length of the pylons
$h_{xy}$	Non-dimensional frequency dependent lift-and moment coefficients ( $x = p, m$ and $y = u, \theta$ )
$I, I_0$	Moment of inertia, Referential moment of inertia
$I_{xx}, I_{yy}$	Moment of inertia about strong axis, weak axis
$I_{zz}$	St.Venant torsional inertial constant
$J$	Mass moment of inertia per unit length of bridge girder plus cables
$J_b$	Mass moment of inertia per unit length of bridge girder
$j_i$	Referring to bending mode ( $i = 1, 2, \dots$ )
$k_i$	Referring to torsional mode ( $i = 1, 2, \dots$ )
$L, L_0$	Length of main span of up-scaled models, Length of main span of referential bridge
$L_s$	Length of side span
$m, m_j$	Moment load per unit length in $z$ -direction; Modal mass of the $j$ th mode
$p, \mathbf{p}$	Load per unit length in $y$ -direction, Load vector per unit length
$q_j, \mathbf{Q}_j$	Modal coordinate of the $j$ th mode, Modal coordinate vector
$u, \mathbf{u}$	Displacement in $y$ -direction, Displacement vector in $y$ -direction
$V$	Vertical reaction force; Mean wind velocity
$V_c$	Critical Euler buckling force; Critical mean wind velocity

## INTRODUCTION

### 1.1 Problem formulation

The work conducted in this thesis deals with the procedure to investigate the aerodynamic stability of long-span suspended bridges. As known nowadays, suspended bridges are one of the primary solutions to overcome the challenge of connecting two points largely distanced.

In opposition to the well known design procedures, suspended bridges have a significant challenging detail - the aerodynamic stability. The seek for longer spans, slender and flexible structures, and streamlined cross-sections, turns the topic of aerodynamic stability a priority focus during design processes.

Since 1940, when the failure of Tacoma Narrow Bridge occurred, the study of aeroelastic effects in bridges has been increasing in order to fully understand how and in which circumstances, the vertical oscillations can couple with torsional oscillations.

The traditional approach to aeroelastic stability of suspension bridges has been based on wind tunnel experiments of a scaled model of the bridge section. The bridge section is undergoing harmonically varying vertical and torsional motions and the aeroelastic induced load and moment load on the bridge section is measured. The idea is to determine the so-called flutter derivatives, which are merely the real and imaginary parts of the frequency response functions of the indicated load components. The flutter derivatives are assumed to be independent of Reynolds number and dependent on the angular frequency and the mean wind velocity via a combined non-dimensional parameter called the reduced frequency. The Reynolds number for onset of flutter in the prototype is supercritical, corresponding

to turbulent boundary layer flows, whereas merely subcritical levels of Reynolds number can be achieved in the model testing. In this thesis, the scaling problem is circumvented by calculating the frequency response functions by means of CFD.

Following the bridge engineering trend, the present thesis look into the aerodynamic stability of suspended bridges up to a main span of 4000m, aiming to evaluate how sensitive the flutter phenomenon can be, when dealing with such systems.

## 1.2 Methodology

Due to the complexity of the topic of the present thesis, involving significant amount of mathematical work, numerical solutions are required. The author chose to use the commercial software as:

- *MatLab* to perform all the mathematical calculations, graphical plot outputs, and solving the required algorithms;
- *ABAQUS* for the structural dynamic analysis, where the eigenfrequencies and mode shapes are obtained from;
- *STAR-CCM+* for the CFD analysis.

Preliminary to this thesis, the author had extensively used *MatLab*, experience which was useful to the work performed in here. However, knowledge of *ABAQUS* was very limited to a much simpler problems and structures, and *STAR-CCM+* was completely unknown to the author. Those factors played an important role on the timeline of the thesis, since an extensive research was needed.

## 1.3 Thesis content

The work presented in this thesis is divided into six main chapters, ordered in the natural way of how the topic is studied, where each chapter complements the next one.

Chapter 1 introduces the reader to the topic of the thesis. Information about how the research is developed is also presented along. The definition of the referential and up-scaled systems, and the scaling assumptions taken into account can be seen in this Chapter.

Chapter 2 deals with the bridge component which plays an important role in the structural dynamic behaviour of the suspended bridges - the cable system. Here, a mathematical formulation for the cable geometry is performed, aiming to determine the horizontal forces

applied, fulfilling the equilibrium state. The results obtained from Chapter 2 are the baseline for the numerical model performed in Chapter 3.

Chapter 3 focus on the structural dynamics behaviour of the structure. The purpose of this chapter is to evaluate the eigenfrequencies and mode shapes of the referential bridge and up-scaled models. A full description of the type of FEM model used, as well as, parameters taken into account is also found along this Chapter. Chapter 3 ends with a validation of the model against reference values and an overview of the results for each case studied.

Chapter 4 is dedicated to the suggested theory to evaluate the frequency response function for the modes of interest, i.e., the modes the author assumes a possible onset of flutter.

Chapter 5 provides the evaluation of the aerodynamic parameters by means of CFD simulations and numerical solutions. A description of the model used for this thesis, together with the chosen parameters can be found here. A description of the different cases studied accompanying with the outcome from each one is presented. The aim core of this Chapter is to validate the theory presented along Chapter 4 and to present results for a set of different variable parameters. A procedure for further numerical evaluation of the critical values of the reduced frequency and wind velocity end this Chapter.

A discussion of the outcomes and recommendations for future frameworks are described in Chapter 6.

## 1.4 Reference bridge and up-scaled models

The reference bridge chosen for this thesis is the East Bridge, a 6790m long bridge composed by two approach bridges and a suspended bridge with length of 2694m (535 + 1624 + 535m). The East Bridge is part of the Great Belt Link, located in Denmark, and connecting the regions of Sjælland and Fyn. The focus is only in the suspended span (main span and two side spans), and, for simplicity, the reference bridge is named along this thesis as Great Belt Bridge.

In order to predict future bridge engineering developments, three up-scaled models are subject of the investigations as follows:

- Main suspended span of 2000m (ahead named as Model A)
- Main suspended span of 3000m (ahead named as Model B)
- Main suspended span of 4000m (ahead named as Model C)

## 1.5 Scaling assumptions

In order to up-scale the models, some assumptions are made as follows.

### Cross sectional area of cables

As reference value, the allowable stress on the cables is calculated for the Great Belt Bridge using Eq.(1.1).

$$\sigma_0 = \frac{H_0}{2 \cdot A_c} \approx 469 \text{ MPa} \quad (1.1)$$

It is assumed that the up-scaled models should fulfil the same criteria of allowable stress. Inserting Eq.(2.4) into Eq.(1.1), the unknown value of  $A_c$  can be determined as

$$\sigma_0 = \frac{\frac{1}{8} \cdot g \cdot (\mu_b + 2 \cdot A_c \cdot \rho_c) \cdot \frac{L_0}{h_0} \cdot L}{2 \cdot A_c} \quad (1.2)$$

where the parameter  $L$  is given, respectively, by 2000, 3000 and 4000m, and the parameter  $\frac{h_0}{L_0}$  is constant and equal to 1/9, representing the sag ratio in the referential bridge. The results are presented in Table 1.1.

Table 1.1 Up-scaled values for cross section area of cables

$L$ [m]	$A_c$ [m <sup>2</sup> ]
1624	0.410
2000	0.566
3000	1.237
4000	3.037

reference values

### Length of side span

The length of the side span is geometrically scaled based on the assumption that the ratio between the pylons height and the main span length is kept. Table 1.2 shows the values considered for the up-scaled models.

Table 1.2 Up-scaled values for side span length

$L$ [m]	$h$ [m]	$L_s$ [m]
1624	180.50	535
2000	222.22	659
3000	333.33	988
4000	444.44	1318

reference values

### Pylons

Following the scaling assumption of keep the ratio between the pylons height and the main span length, the up-scaled pylon height is determined by the cable calculations. In order to obtain a realistic result, the section of the pylons is also up-scaled.

The inertial moment  $I$  of the pylon legs are determined, so the reaction force  $V$  on the pylons from the cables in proportion to the critical Euler buckling force  $V_c$  is the same for the referential configuration and the up-scaled bridges.

$V$  is varying as  $(\mu_b + 2 \cdot \mu_c) \cdot L$ , and  $V_c$  as  $\frac{I}{L^2}$  for the up-scaled bridges. Hence,

$$\frac{V}{V_c} = \frac{V_0}{V_{c,0}} \Rightarrow \frac{I}{I_0} = \frac{(\mu_b + 2 \cdot \mu_c) \cdot L^3}{(\mu_b + 2 \cdot \mu_{c,0}) \cdot L_0^3} \quad (1.3)$$

where  $V_0$  and  $V_{c,0}$  indicates the reaction force and critical buckling load of the referential configuration with the inertial moment  $I_0$  and free span  $L_0$ .  $\mu_c$  and  $\mu_{c,0}$  indicate, respectively, the cable mass per unit length of the up-scaled and referential bridge. The mass per unit length  $\mu_b$  is assumed the same for the referential and the up-scaled bridge.

The geometric location of the cross beams is, however, kept adopting the same reference distances as in the Great Belt Bridge. It is assumed that this detail do not influence the results. Figure 1.1 shows the critical buckling length of the pylons. In the Models B and C, due to the significant increase of the distance between cross beams, an additional cross beam is placed at half of the distance (in Model B) and two cross beams at one third and two thirds of the distance (in Model C).

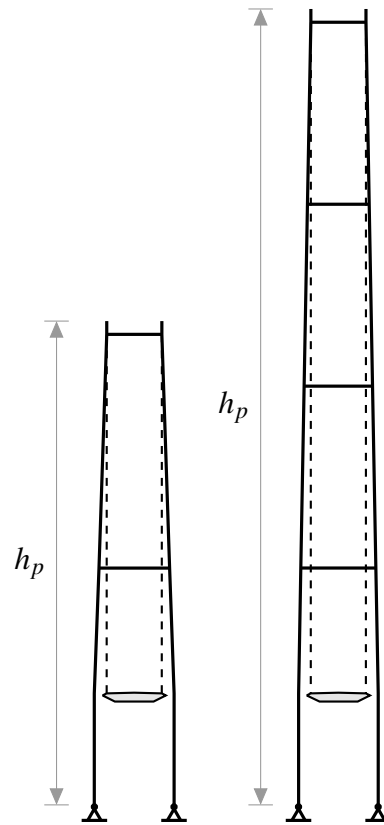


Fig. 1.1 Up-scaling of pylons

### Damping ratios

The damping ratios considered in the dynamic analysis of the up-scaled models, are the same of the reference values mentioned on Table 3.4 on Section 3.3.

## CABLE GEOMETRY

*It is known that cables are an important element regarding the aerodynamic stability of suspended bridges. As structural element, cables are usually assumed to be fully flexible in bending. In order to be able to possess transverse stiffness, a cable should have an axial force. The purpose of this Chapter is to determine the axial force on the cables of the reference bridge, as well as, for the investigated up-scaled models.*

### 2.1 Cable elements formulation

Along this Section, the analytical approach used to calculate the horizontal force  $H$  is described, along with the iterative process needed to solve the problem. The formulation is divided into two parts: the main span, where symmetry is used meaning to solve from the middle point of the suspended span until the top of the pylon, and the side span, from the anchor blocks to the top of the pylon.

#### 2.1.1 Main span

The initial calculations are based on the data from the reference bridge ([5] and [8]), and are as follows:

- $L = 1624$  m
- $h = 180.5$  m

- $\mu_b = 14.78 \cdot 10^3 \text{ kg/m}$
- $\mu_c = 3.36 \cdot 10^3 \text{ kg/m}$
- $dx = 24 \text{ m}$

The spatial discretization along  $x$ -axis, has origin at the symmetry point of the cable, and along  $y$ -axis is oriented in the upwards direction. As seen in Appendix A, the hangers are not equally distributed near the pylons and at the centre of the suspended bridge. Due to the fact this is not a relevant parameter which influences the dynamic analysis, the distance between hangers is defined in a way to create equal elements from pylon to pylon.

The statical model for the main span is described in Figure 2.1.

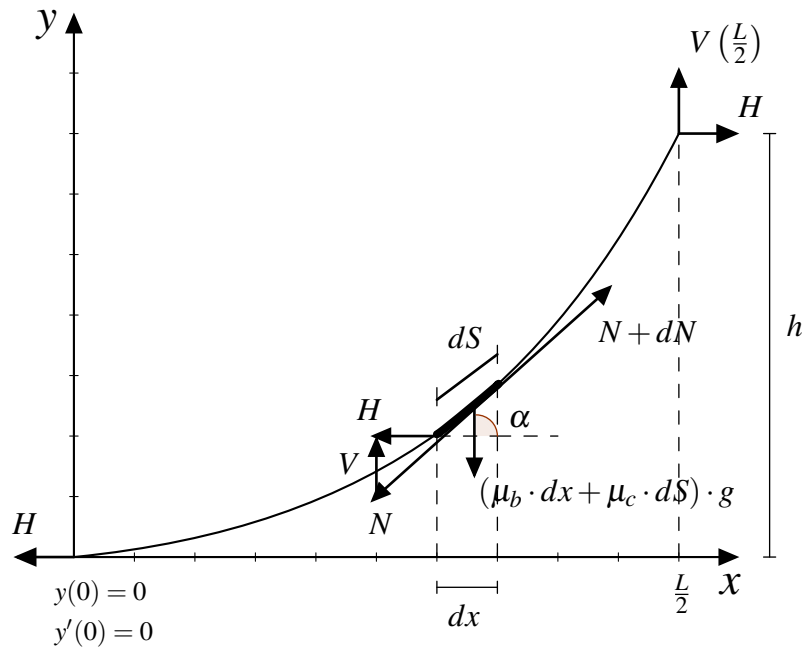


Fig. 2.1 Main span statical model

From Figure 2.1 the equations below can be determined:

$$V = H \cdot \tan(\alpha) = H \cdot \frac{dy}{dx} \quad (2.1)$$

$$dS = \sqrt{1 + \left(\frac{dy}{dx}\right)^2} dx \quad (2.2)$$

Since there are no horizontal external loads, the horizontal component  $H$  of the normal force is constant.

Using Eq.(2.1) and Eq.(2.2) it is possible to define the following equality:

$$\begin{aligned} \frac{dV}{dx} = H \cdot \frac{d^2y}{dx^2} = \mu_b \cdot g + \mu_c \cdot g \cdot \sqrt{1 + \left(\frac{dy}{dx}\right)^2} \Rightarrow \\ \frac{d^2y}{dx^2} - \frac{g}{H} \cdot \left( \mu_b + \mu_c \cdot \sqrt{1 + \left(\frac{dy}{dx}\right)^2} \right) = 0 \quad x \in \left] 0, \frac{L}{2} \right] \end{aligned} \quad (2.3)$$

Eq.(2.3) defines the equilibrium to be fulfilled along the iteration. For the main span the boundary conditions are defined as:

- $y(0) = 0$
- $\frac{d}{dx} y(0) = 0$

To start the iteration process an initial value  $H_0$  of  $H$  is needed. This is obtained from a parabolic suspension so  $dS = dx$ .

$$H_0 = \frac{1}{8} \cdot g \cdot (\mu_b + \mu_c) \cdot \frac{L^2}{h} \quad (2.4)$$

After each iteration with a present solution for  $y(x)$ , a new value of  $H_1$  is obtained from Eq.(2.5).

$$H_1 = \frac{g}{h} \cdot \int_0^{\frac{L}{2}} \left( \frac{L}{2} - x \right) \cdot \left( \mu_b + \mu_c \cdot \sqrt{1 + \left(\frac{dy}{dx}\right)^2} \right) dx \quad (2.5)$$

The iteration process is terminated when  $H_1$  deviates insignificantly from the previous iterated value  $H_0$ , corresponding to the criteria  $\left| \frac{H_1}{H_0} - 1 \right| < 10^{-6}$ .

In order to solve Eq.(2.3) numerically, the ODE is represented in a state vector formulation

$$\begin{cases} \frac{d}{dx} \mathbf{Z}(x) = \mathbf{g}(\mathbf{Z}(x)) \\ \mathbf{Z}(0) = \mathbf{0} \end{cases} \quad (2.6)$$

and solved by means of a Runge-Kutta 4th order scheme, as shown below.

$$\mathbf{Z}(x) = \begin{bmatrix} y(x) \\ \frac{dy(x)}{dx} \end{bmatrix}, \quad \mathbf{g}(x) = \begin{bmatrix} \frac{dy(x)}{dx} \\ \frac{g}{H} \cdot \left( \mu_b + \mu_c \cdot \sqrt{1 + \left(\frac{dy}{dx}\right)^2} \right) \end{bmatrix} \quad (2.7)$$

The procedure described above is inserted in MatLab and the algorithm is illustrated in the flowchart shown in Figure 2.2.

The updating of  $y(x)$  described in Figure 2.2 is determined based on Eq.(2.8).

$$\begin{aligned} y_1(x) &= y(x) + \Delta y(x) \\ \Delta y(x) &= 4 \cdot \frac{x^2}{L^2} \cdot \left( h - y\left(\frac{L}{2}\right) \right) \end{aligned} \quad (2.8)$$

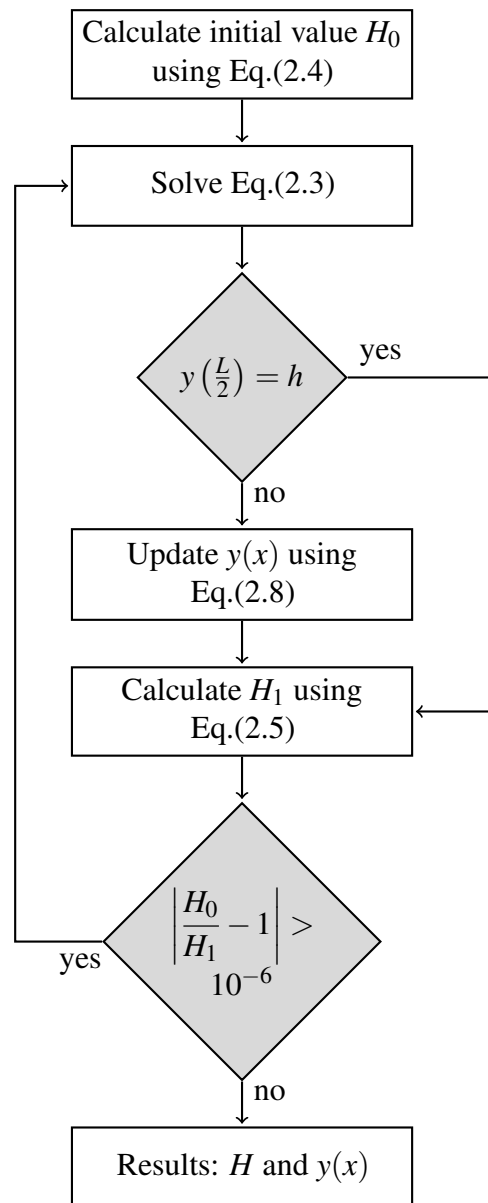


Fig. 2.2 Flowchart of the algorithm for main span

### 2.1.2 Side span

After analysing the main span, the value of  $H$  is known, however, the slope of the cables at the anchor blocks is unknown. The calculations procedure for the side spans are, in general, similar to the ones described along Section 2.1.1. The following parameters apply:

- $L_s = 535$  m
- $\mu_c = 3.45 \cdot 10^3$  kg/m

Figure 2.3 shows the statical model considered for the side span.

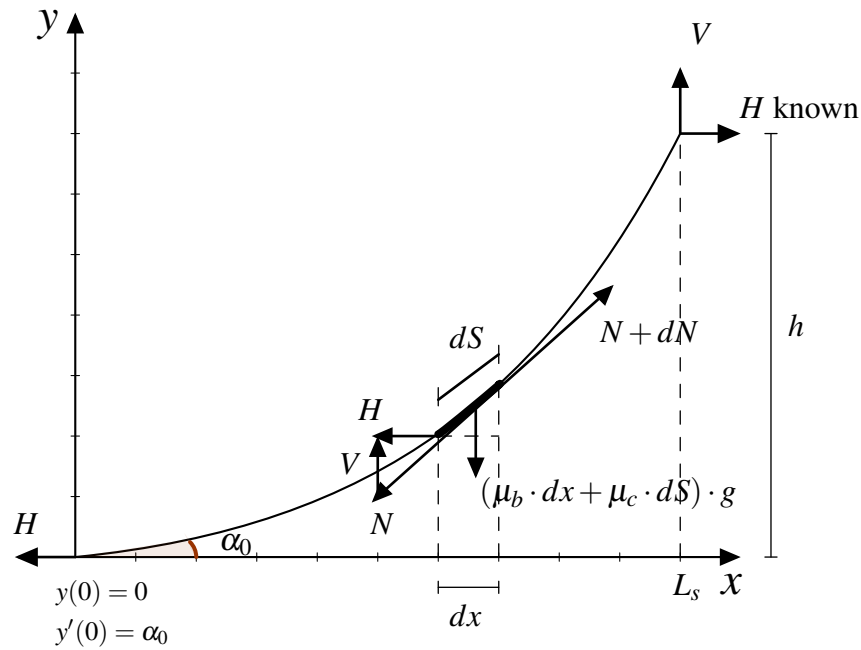


Fig. 2.3 Side span statical model

Similarly to previous procedure, an initial estimation of the slope (see Eq.(2.10)) can be obtained based on parabolic suspension.

$$H \cdot \frac{d^2y}{dx^2} - (\mu_b + \mu_c) \cdot g = 0 \Rightarrow$$

$$y(x) = \alpha_0 \cdot x - \frac{1}{2} \cdot \left( \frac{\mu_b + \mu_c}{H} \right) \cdot g \cdot x^2 \quad (2.9)$$

$$y(L_s) = h = \alpha_0 \cdot L_s - \frac{1}{2} \cdot \left( \frac{\mu_b + \mu_c}{H} \right) \cdot g \cdot L_s^2 \Rightarrow$$

$$\alpha_0 = \frac{2 \cdot H \cdot h + (\mu_b + \mu_c) \cdot g \cdot L_s^2}{2 \cdot H \cdot L_s} \quad (2.10)$$

Eq.(2.3) is now possible to solve introducing the boundary conditions as follows, within the interval of  $x \in [0, L_s]$ :

- $y(0) = 0$
- $\frac{d}{dx} y(0) = \alpha_0$

A flowchart of the algorithm for the side span is shown in Figure 2.4. The updating of  $\alpha_0$  described in Figure 2.4 is determined based on Eq.(2.11), assuming that the increment  $\Delta\alpha_0$  is proportional to the deviation of  $y(L_s)$  in proportion to  $h$  (case of parabolic suspension).

$$\begin{aligned} \alpha_0 &= \alpha_0 + \Delta\alpha_0 \\ \Delta\alpha_0 &= \frac{h - y(L_s)}{L_s} \end{aligned} \quad (2.11)$$

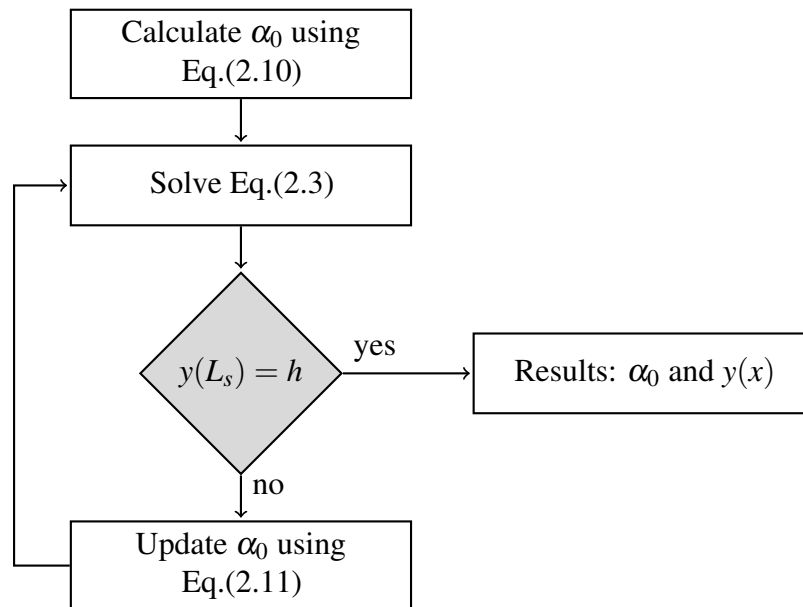


Fig. 2.4 Flowchart of the algorithm for side span

Finalized the procedure and all values acquired, one can determine the vertical force on the pylons  $V$  from each cable, by means of Eq.(2.12).

$$V = H \cdot \left. \frac{dy}{dx} \right|_{x=L_s} \quad (2.12)$$

## 2.2 Results

The procedure described in Sections 2.1.1 and 2.1.2 is initially performed for the data from the Great Belt Bridge (main span of 1624m and side span of 535m). The results are validated using equilibrium state between the vertical forces at the pylons and anchor blocks, and the self-weight of the structure (see Eq.(2.13)).

$$2 \cdot \underbrace{(V_{anchor} + V_{pylon})}_{\text{values from Eq.(2.12)}} = \underbrace{\mu_b \cdot (L + 2 \cdot L_s) \cdot g}_{\text{bridge girder}} + \underbrace{2 \cdot \mu_c \cdot L_c \cdot g}_{\text{cables main span}} + \underbrace{4 \cdot \mu_c \cdot L_{cs} \cdot g}_{\text{cables side span}} \quad (2.13)$$

The algorithm is then run changing the parameters  $L$ ,  $L_s$  and  $\mu_c$  for the up-scaled models, according the assumptions described in Section 1.5. The results for main and side spans can be seen, respectively, in Figures 2.5 and 2.6.

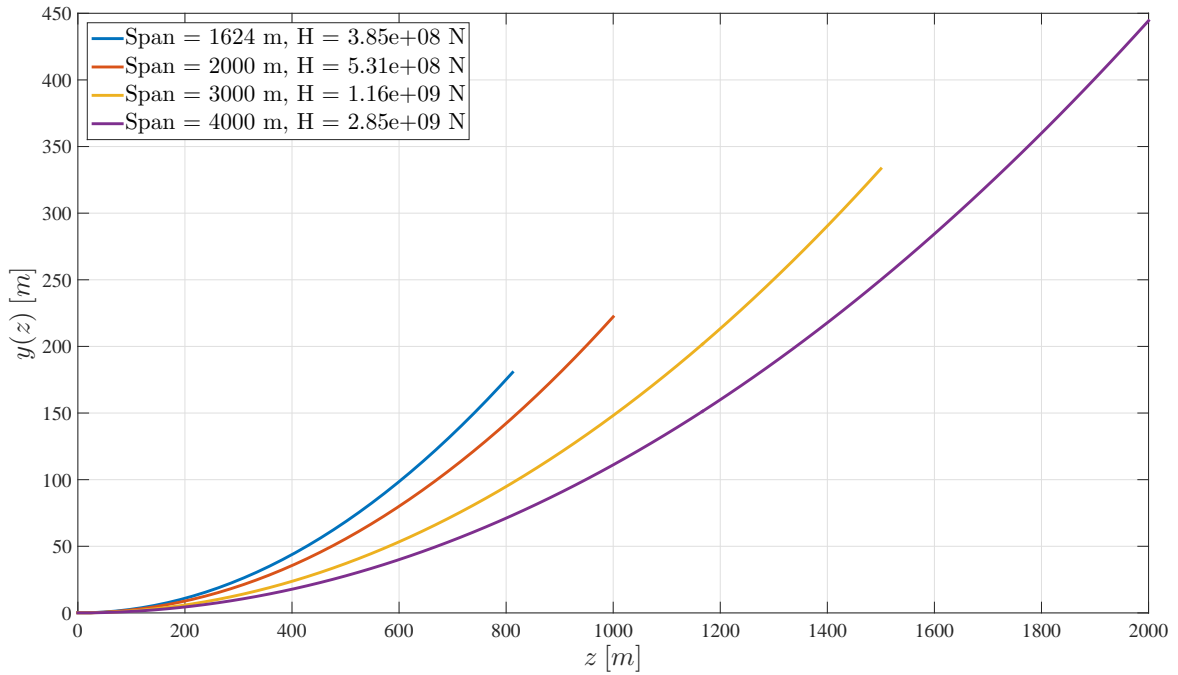


Fig. 2.5 Equilibrium suspension of cables in main span

The horizontal spacing for the hangers,  $dx$ , varies between models, in order to fulfil the criteria of equal amount of hangers with a spacing of order of magnitude close to 24 m.

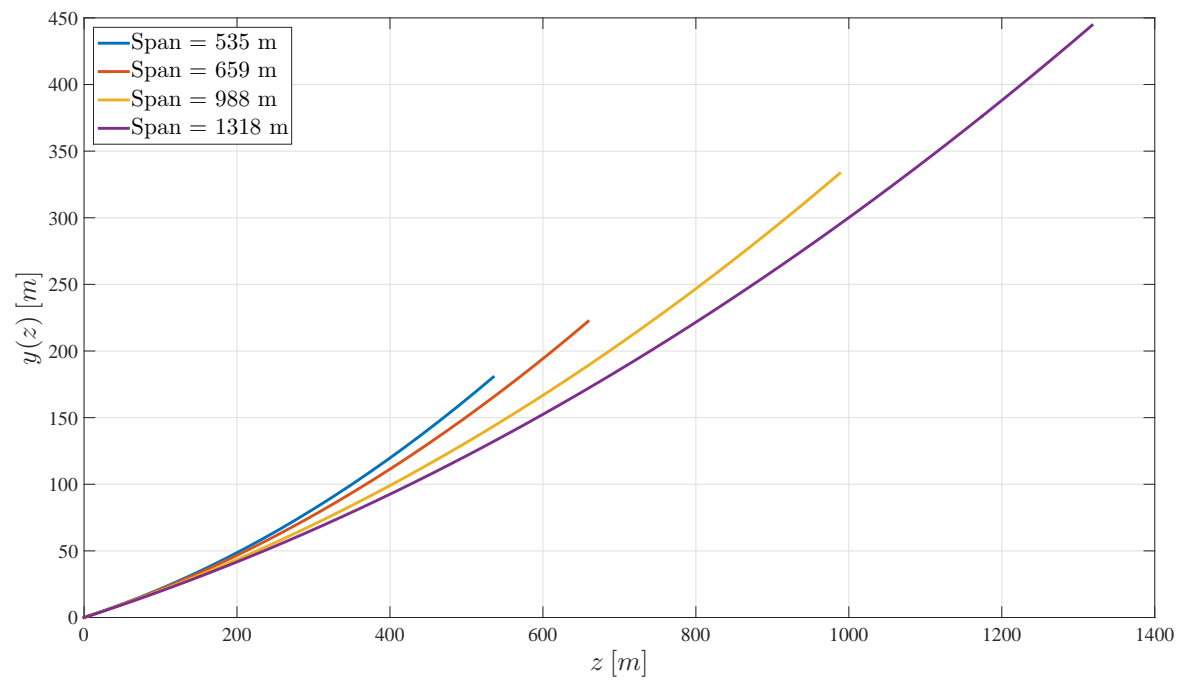


Fig. 2.6 Equilibrium suspension of cables in side span

## STRUCTURAL DYNAMICS

*In order to evaluate the structural response of the bridge models, a finite element model is created using ABAQUS software. The outputs requested are the eigenfrequencies and mode-shapes. The choice of ABAQUS lays on the fact that this software is able to solve advanced non-linear static and dynamic problems. In the particular case of suspended bridges, the most important non-linearity is the geometrical stiffness in the cable system.*

### 3.1 Description of the model

In order to keep the duration of the simulations within reasonable time frame, as well as, being able to run it with the computational power available, the model is build using simple Bernoulli-Euler beam elements.

The cable system and hangers are defined by beam elements with low bending stiffness. The girder is modelled as a beam element placed in the centroid of the section and spanning between hangers. Transversally, the beam elements of the girder are connected to the hangers using kinematic coupling, an *ABAQUS* tool which allow to constrain the DOF's of a master node (girder) in relation to slave nodes (hangers). The pylons are modelled as box elements, with equivalent section as described in the drawings in Appendix A. As by default in *ABAQUS* software, the coordinate system adopted is illustrated in Figure 3.1. The cardinal directions are also represented, as a close approximation to the orientation of the Great Belt Bridge.

In the following, the definition of the Cartesian referential system  $(x, y, z)$  is changed. Now the origin of the coordinate system is chosen at the end of the bridge, the  $z$ -axis is

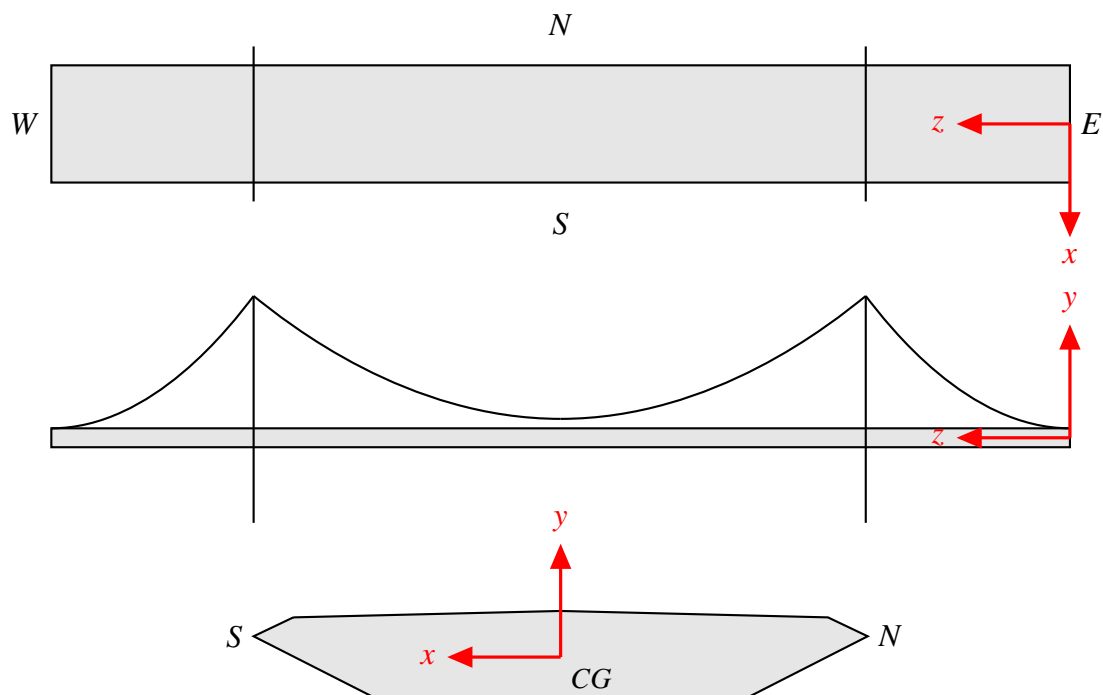


Fig. 3.1 Coordinate system and model orientation

placed along the bridge girder orientated toward the opposite end, and the  $y$ -axis is orientated in the vertical direction.

For the sake of simplicity, and taking into account that this detail do not significantly influence the results, the bridge deck is modelled horizontally, without camber, as seen in the longitudinal section on Figure 3.1.

## 3.2 Material properties

The structure is mainly composed by two different materials: steel and reinforced concrete. It is known, according [5], that the steel is class S355 J2. Material properties considered along all the components are shown on table A.

### 3.2.1 Cable system

The section properties for the different elements are based on literature - [5] and [8]. For the sake of simplicity, the cables are modelled with the section properties from the main span, although the cables on side spans has slightly different parameters. It is assumed that the cables do not have significant bending and torsional stiffness. The cross sectional area,

Table 3.1 Material properties

Properties	Value	Units
$E_{steel}$	$2.1 \cdot 10^{11}$	Pa
$\nu_{steel}$	0.3	[-]
$\rho_{steel}$	7850	kg/m <sup>3</sup>
$E_{concrete}$	$4.0 \cdot 10^{10}$	Pa
$\rho_{concrete}$	2400	kg/m <sup>3</sup>
$\nu_{concrete}$	0.2	[-]

$A_c$ , is equal to 0.41 m<sup>2</sup> and the mass per unit length,  $\mu_c$ , is equal to  $3.36 \cdot 10^3$  Kg/m for the referential bridge.

### 3.2.2 Hangers

According [5], the cables are connected to the girder by two parallel hangers with a distance between each other of half meter. In order to simplify the modelling process, only one hanger is modelled but its section properties are doubled. In similarity to the cable system, also the hangers are modelled without significant bending and torsional stiffness. The cross sectional area,  $A_h$ , and density,  $\rho_h$ , are, respectively, equal to  $6.5 \cdot 10^{-2}$  m<sup>2</sup> and 7850 Kg/m<sup>3</sup>.

### 3.2.3 Pylons

The two existing pylons are divided into four different components: two vertical elements and two cross beams. The vertical elements consist in a box shape with regular geometry constant from the foundation until the level of the bridge girder and a different one from there until the top. The two cross beams, placed at project defined level, has also two different cross sections. All the element components of the pylons are modelled as Bernoulli-Euler beam elements. The sectional dimensions of these elements are described in Table 3.2.

Table 3.2 Sectional properties of the pylons (referential bridge)

Element	$a$ [m]	$b$ [m]	$t$ [m]
Lower section leg	13.8	15.1	1.7
Upper section leg	8.0	9.0	1.7
Lower cross beam	9.0	12.0	1.2
Upper cross beam	9.0	13.0	0.8

(Notation: refer to Figure 3.2)

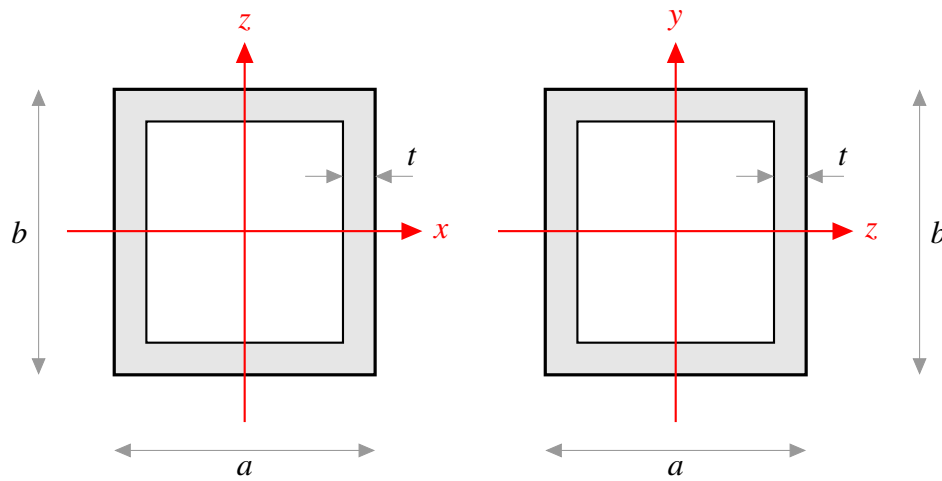


Fig. 3.2 Notation for section properties of pylons  
(Left side: pylon legs; Right side: cross beams)

### 3.2.4 Bridge girder

As stated in Section 3.1, the model is based in simple elements due to faster simulation time and to the fact that the chosen elements perform results according expected. Following this approach, the bridge girder is modelled using Bernoulli-Euler beam elements.

The mass moment of inertia per unit length of the bridge deck becomes

$$J_b = \rho \cdot (I_{xx} + I_{yy}) \quad (3.1)$$

where  $I_{xx}$  and  $I_{yy}$  indicates, respectively, inertial moment about the strong and weak axis.

Regarding the bridge girder, the beam elements are modelled based on the parameters founded in [5], [8] and in the data in Appendix B. Table 3.3 shows the parameter taken into account.

Table 3.3 Section properties for bridge girder

Properties	Value	Units
$A_b$	1.137	m <sup>2</sup>
$I_{yy}$	3.577	m <sup>4</sup>
$I_{xx}$	94.694	m <sup>4</sup>
$I_{zz}$	9.366	m <sup>4</sup>
$J_b$	$1.277 \cdot 10^6$	Kg.m
$\mu_b$	$14.78 \cdot 10^3$	kg/m

The parameter  $I_{zz}$  indicates the St.Venant torsional inertial constant.

### 3.3 Model validation

In order to assure the reliability of the model outputs, the results from eigenfrequencies for bending and torsional vibrations are compared against reference values, as well as, crude analytical solutions.

An analytical solution for the fundamental angular frequency for shallow cables is founded in [7], and shown in Eq.(3.2). The mass per unit length,  $m$ , is determined by summing the contribution from the girder and cables. The mass per unit length from the hangers is neglected, assuming a rigid connection between girder and cables, thus an upper bound solution is expected, [7].

$$\omega_1 = 8.99 \cdot \sqrt{\left(\frac{H}{m \cdot L^2}\right)} \quad (3.2)$$

When computing Eq.(3.2) with the parameters from the Great Belt Bridge, the fundamental bending frequency is estimated as follows:

$$f_1 = \frac{8.99 \cdot \sqrt{\left(\frac{3.85 \cdot 10^8}{21.5 \cdot 10^5 \cdot 1624^2}\right)}}{2 \cdot \pi} \approx 0.12 \text{ Hz} \quad (3.3)$$

An operational modal analysis was performed in 1999 and the results obtained using the software *ARTEMIS* published one year later in [1]. The results shown in Table 3.4 are the ones obtained using the solver SCI-UPC (Stochastic Subspace Identification techniques), which the author assumes to represent the most accurate ones, based on the advanced techniques involved in the outputs.

Table 3.4 Reference values from modal analysis

Mode $j$	Symmetry	$f$ [Hz]	$\zeta$ [%]
1	S	0.113	0.90
2	SS	0.174	1.25
3	S	0.208	0.79
4	SS	0.241	0.44
5	S	0.287	0.20
6	S	0.332	1.25
7	SS	0.372	0.80
8	SS	0.391	0.68
9	S	0.429	1.49

The labels S and SS on Table 3.4 and 3.5 indicate symmetric and skew-symmetric modes, respectively. Based on the scaling assumptions from Section 1.5, the damping ratios  $\zeta$  (in %) cited on Table 3.4 will be used for the up-scaled models.

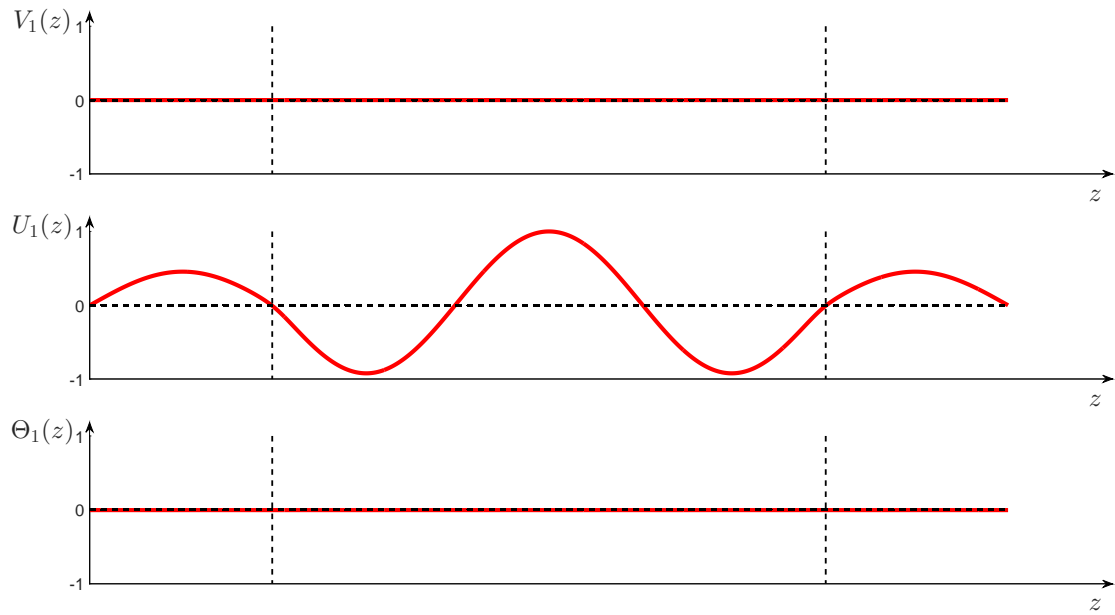
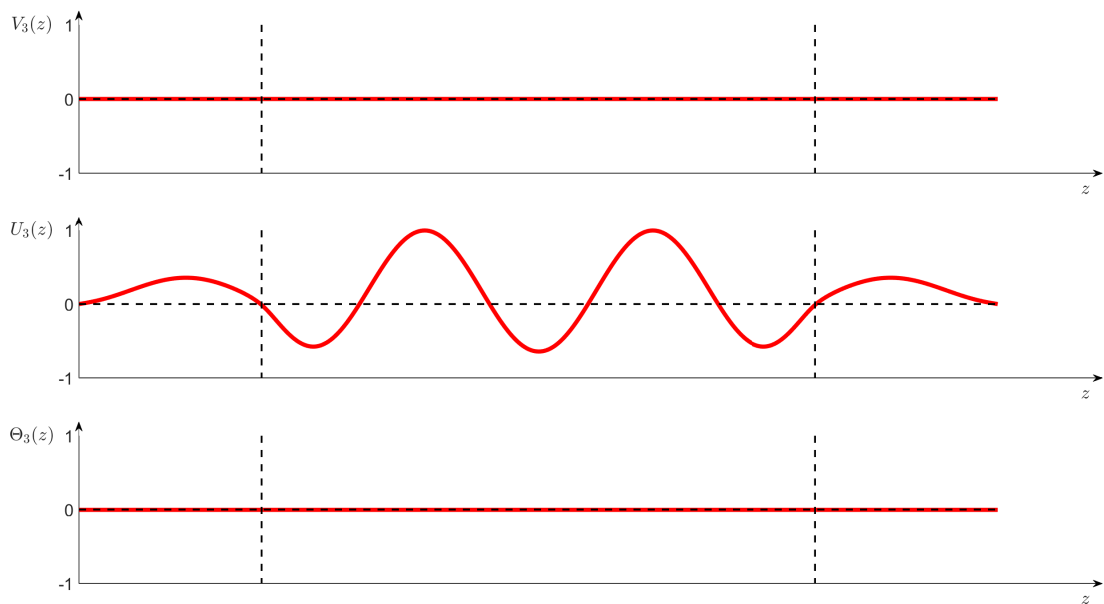
### 3.4 Outputs from dynamic analysis

As output of the dynamic analysis performed in *ABAQUS*, the parameters of interest are extracted as, the bending and torsional eigenmodes and corresponding eigenfrequencies associated to each mode. As stated in Section 1.5, the damping ratios are the ones from the reference values in Table 3.4.

The results are shown in Table 3.5 and a plot of the selected mode shapes for the referential bridge can be seen in Figures 3.3 to 3.6, where  $V_i(z)$ ,  $U_i(z)$  and  $\Theta_i(z)$  represent the normalized amplitudes of the eigenvector function.

Table 3.5 Eigenfrequencies for referential and up-scaled bridges

Mode	Great Belt		Model A		Model B		Model C	
	Symm.	$f$ [Hz]	Symm.	$f$ [Hz]	Symm.	$f$ [Hz]	Symm.	$f$ [Hz]
1	S	0.128	S	0.113	S	0.090	S	0.078
2	SS	0.174	SS	0.151	SS	0.119	S	0.083
3	S	0.216	S	0.187	S	0.129	SS	0.103
4	SS	0.269	S	0.243	SS	0.148	SS	0.115
5	S	0.294	SS	0.277	SS	0.180	S	0.128
6	SS	0.306	S	0.318	SS	0.183	SS	0.156
7	S	0.331	SS	0.323	S	0.215	S	0.171
8	SS	0.387	SS	0.361	S	0.217	S	0.185
9	S	0.438	S	0.390	SS	0.242	SS	0.211

Fig. 3.3 First symmetric bending mode  $j = 1$  (referential bridge)Fig. 3.4 Second symmetric bending mode  $j = 3$  (referential bridge)

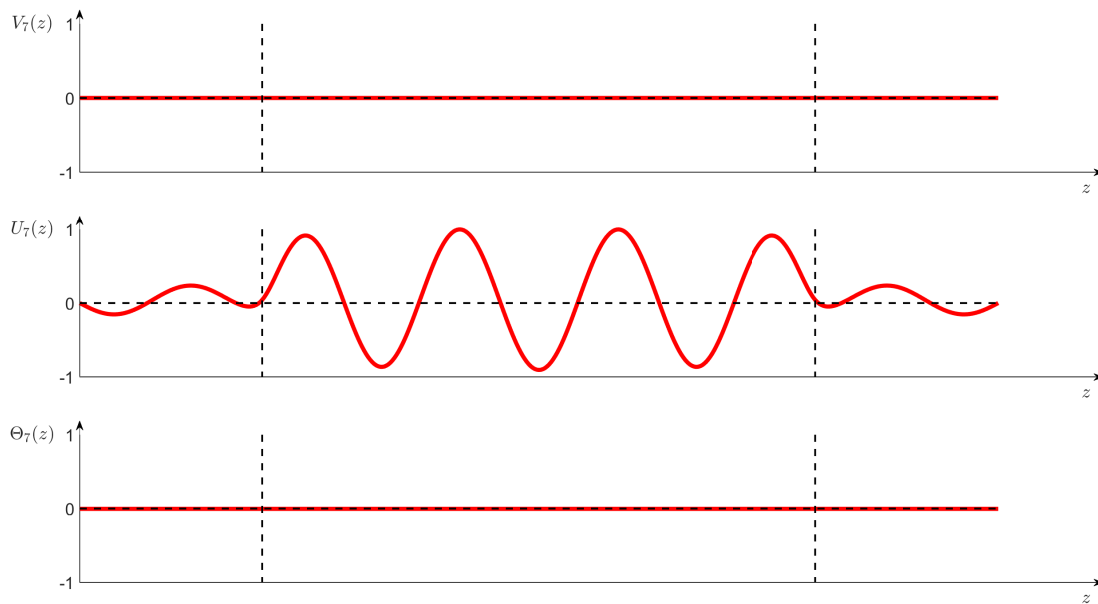


Fig. 3.5 Third symmetric bending mode  $j = 7$  (referential bridge)

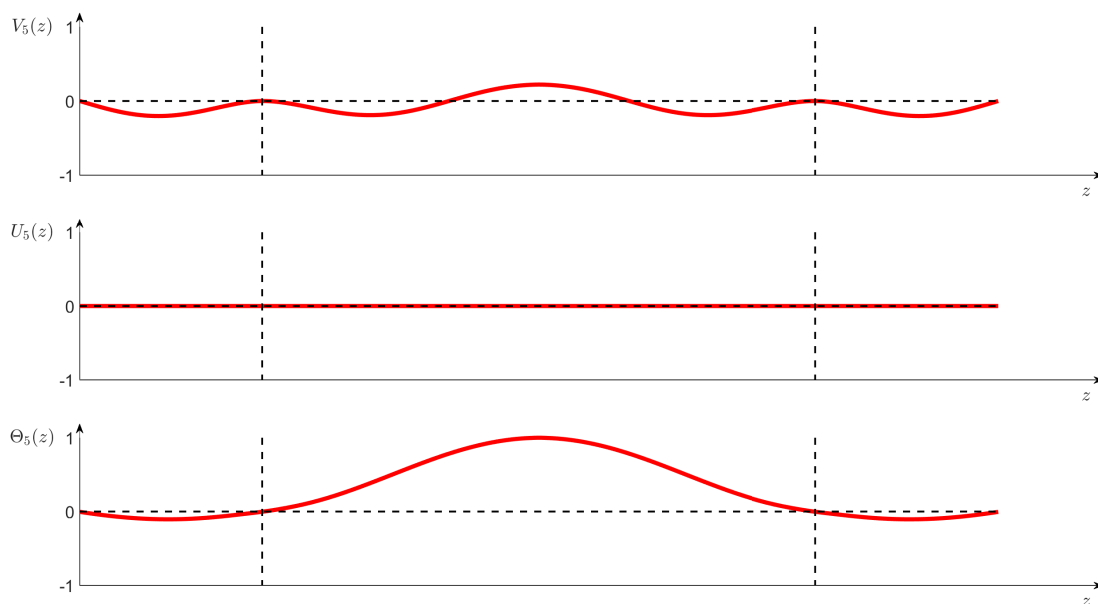


Fig. 3.6 First symmetric torsional mode  $j = 5$  (referential bridge)

The non-dimensional quantities  $a_{jj}$ ,  $a_{kk}$  and  $a_{jk}$  from Eq.(4.34) are evaluated numerically for the referential bridge and up-scaled models. Table 3.6 shows the results considering the

onset of flutter between the first symmetrical bending mode  $j_1$  and the first symmetrical torsional mode  $k_1$ , for the referential bridge and Model C (4000m suspended span).

Table 3.6 Non-dimensional quantities  $a_{jk}$

	Great Belt Bridge	Model C
$\mu$	$21.5 \cdot 10^3 \text{ kg/m}$	$64.5 \cdot 10^3 \text{ kg/m}$
$J$	$2.9 \cdot 10^6 \text{ kg.m}$	$13.2 \cdot 10^6 \text{ kg.m}$
$a_{jj}$	0.308	0.345
$a_{kk}$	0.239	0.161
$a_{jk}$	0.038	0.178
$\frac{a_{jk}}{a_{jj}}$	0.124	0.515
$\frac{a_{jk}}{a_{kk}}$	0.159	1.101

(results for  $j_1$  and  $k_1$ )

As shown, the non-dimensional quantities corresponding to the normalized eigenmodes are not independent of the up-scaling, neither approximately similar.



## AERODYNAMICS

*The focus of this Chapter is to describe the theory used to obtain the aerodynamic parameters and the frequency response functions. The proposed theory differs from the approach in Scanlan [9] since it considers the different bridge deck response along the bridge and uses normalized non-dimensional quantities. The latter characteristic reveals to be useful when dealing with up-scaled systems. The core of the aerodynamic effects is the onset of flutter.*

### 4.1 Modal analysis

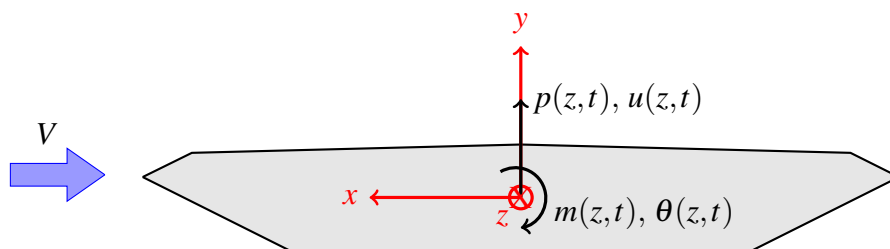


Fig. 4.1 Notation

$u(z, t)$  and  $\theta(z, t)$  signify, respectively, the displacement in the  $y$ -direction and the rotation in the  $z$ -direction of the bridge section at position  $z$  at the time  $t$  from a given static referential deformation.

$p(z, t)$  and  $m(z, t)$  signify, respectively, the work conjugated load per unit length in the  $y$ -direction and the moment load per unit length in the  $z$ -direction at position  $z$  at the time  $t$ .

The loads may be assemble in the vector:

$$\mathbf{p}(z,t) = \begin{bmatrix} p(z,t) \\ m(z,t) \end{bmatrix} \quad (4.1)$$

Flutter is assumed to take place as a modal coupling between the  $j$ th and the  $k$ th eigenmodes. Hence, at the onset of flutter, the displacement field may be written as:

$$\mathbf{u}(z,t) \simeq \mathbf{\Phi}_j(z) q_j(t) + \mathbf{\Phi}_k(z) q_k(t) \quad (4.2)$$

where:

$$\mathbf{u}(z,t) = \begin{bmatrix} u(z,t) \\ \theta(z,t) \end{bmatrix} \quad (4.3)$$

$q_j(t)$  is a modal coordinate, and  $\mathbf{\Phi}_j(z)$  is the related undamped eigenmode vector, given as:

$$\mathbf{\Phi}_j(z) = \begin{bmatrix} U_j(z) \\ \Theta_j(z) \end{bmatrix} \quad (4.4)$$

The eigenmode vector fulfills the orthogonality property:

$$\int_0^L \mathbf{\Phi}_j^T(z) \mathbf{M} \mathbf{\Phi}_k(z) dz = \begin{cases} 0, & j \neq k \\ m_j, & j = k \end{cases} \quad (4.5)$$

where

$$\mathbf{M} = \begin{bmatrix} \mu & 0 \\ 0 & J \end{bmatrix} \quad (4.6)$$

where  $L$  is the total length of the bridge (main span plus side spans), and  $\mu$  is the constant mass per unit length of the bridge deck plus cables and  $J$  is the mass moment of inertia per unit length of the bridge deck plus cables given as:

$$J = J_b + \frac{B^2}{2} \cdot \mu_c \quad (4.7)$$

$m_j$  indicates the modal mass of the  $j$ th mode given as

$$\begin{aligned} m_j &= \int_0^L \mathbf{\Phi}_j^T(z) \mathbf{M} \mathbf{\Phi}_j(z) dz \\ &= \int_0^L (\mu \cdot U_j^2(z) + J \cdot \Theta_j^2(z)) dz \end{aligned} \quad (4.8)$$

Due to the orthogonality property of the eigenmodes, the modal equations of motion decouple. The  $j$ th modal equation reads:

$$m_j \cdot (\ddot{q}_j(t) + 2 \cdot \zeta_j \cdot \omega_j \cdot \dot{q}_j(t) + \omega_j^2 \cdot q_j(t)) = f_j(t) \quad (4.9)$$

where  $\zeta_j$  indicates the structural modal damping ratio,  $\omega_j$  is the undamped angular eigenfrequency, and  $f_j(t)$  is the modal load given as:

$$f_j(t) = \int_0^L \Phi_j^T(z) \mathbf{p}(z, t) dz \quad (4.10)$$

Conveniently, the modal loads may be stores in the vector  $\mathbf{f}(t)$  given as:

$$\mathbf{f}(t) = \int_0^L \Phi^T(z) \mathbf{p}(z, t) dz \quad (4.11)$$

$$\mathbf{f}(t) = \begin{bmatrix} f_j(t) \\ f_k(t) \end{bmatrix} \quad (4.12)$$

$\Phi(z)$  is a modal matrix function given as:

$$\Phi(z) = \begin{bmatrix} \Phi_j(z) & \Phi_k(z) \end{bmatrix} \quad (4.13)$$

## 4.2 Frequency response analysis

Assume that the bridge deck undergoes harmonic varying deformations on the form

$$\mathbf{u}(z, t) = \mathbf{U}(z) \cdot e^{i\omega t} \quad (4.14)$$

where  $i$  indicates the complex unit,  $\omega$  is the angular frequency of the excitation, and  $\mathbf{U}(z)$  is a complex amplitude vector function depending on  $z$ , i.e., a phase difference between the two components may be present. Then, the modal coordinates become harmonic varying as well:

$$\mathbf{q}(t) = \mathbf{Q} \cdot e^{i\omega t} \quad (4.15)$$

$$\mathbf{q}(t) = \begin{bmatrix} q_j(t) \\ q_k(t) \end{bmatrix} \quad (4.16)$$

$$\mathbf{Q} = \begin{bmatrix} Q_j \\ Q_k \end{bmatrix} \quad (4.17)$$

From Eq.(4.2), (4.13), (4.14), (4.15) follows

$$\mathbf{U}(z) = \mathbf{\Phi}(z) \mathbf{Q} \quad (4.18)$$

The pressure over the bridge deck and the load resultants per unit length  $p(z, t)$  and  $m(z, t)$  become harmonic varying as well. Hence, Eq.(4.1) can be written as:

$$\mathbf{p}(z, t) = \mathbf{P}(z, \omega) e^{i\omega t} \quad (4.19)$$

$$\mathbf{P}(z, \omega) = \mathbf{H}_a(\omega, V) \mathbf{U}(z) = \mathbf{H}_a(\omega, V) \mathbf{\Phi}^T(z) \mathbf{Q} \quad (4.20)$$

$$\mathbf{H}_a(\omega, V) = \begin{bmatrix} H_{pu}(\omega, V) & H_{p\theta}(\omega, V) \\ H_{mu}(\omega, V) & H_{m\theta}(\omega, V) \end{bmatrix} \quad (4.21)$$

$\mathbf{H}_a(\omega, V)$  indicates the frequency response matrix for the load per unit length  $p(z, t)$  and the moment load per unit length  $m(z, t)$  due to harmonic varying deformations  $u(z, t)$  or  $\theta(z, t)$  of the bridge deck. E.g.  $H_{p\theta}(\omega, V)$  indicates the frequency response function for  $p(z, t)$ , when the bridge deck undergoes harmonic varying rotation  $\theta(z, t) = \Theta(z) \cdot e^{i\omega t}$  with the vertical displacement  $u(z, t) \equiv 0$ . The frequency response function depend on  $V$  via the Reynolds number  $Re = \frac{V \cdot B}{\nu}$ , where  $\nu$  is the kinematic viscosity. However, this dependency is assumed to be weak, because the boundary layer around the bridge deck is everywhere turbulent, i.e. both the referential and the up-scaled bridges are considered at supercritical values of Reynolds number. Notice that  $\mathbf{H}_a(\omega, V)$  is assumed to be independent of  $z$ . This is necessary in order to apply the results from the 2D CFD analysis. We may refer to  $\mathbf{H}_a(\omega, V)$  as the aeroelastic frequency response matrix.  $\mathbf{H}_a(\omega, V)$  depends on the mean wind speed  $V$  in the negative  $x$ -direction, which is assumed constant along the bridge, see Figure 4.1.

The modal loads become harmonic varying as well. Then Eq.(4.12) may be written as:

$$\mathbf{f}(t) = \mathbf{F}(\omega, V) \cdot e^{i\omega t} \quad (4.22)$$

where the amplitude vector follows from Eq.(4.11), (4.19), (4.20) as

$$\mathbf{F}(\omega, V) = \int_0^L \mathbf{\Phi}^T(z) \mathbf{P}(z, \omega, V) dz = \mathbf{A}_a(\omega, V) \mathbf{Q} \quad (4.23)$$

where:

$$\begin{aligned} \mathbf{A}_a(\omega, V) &= \int_0^L \boldsymbol{\Phi}^T(z) \mathbf{H}_a(\omega, V) \boldsymbol{\Phi}(z) dz \\ &= \int_0^L \begin{bmatrix} \boldsymbol{\Phi}_j^T(z) \\ \boldsymbol{\Phi}_k^T(z) \end{bmatrix} \begin{bmatrix} H_{pu}(\omega, V) & H_{p\theta}(\omega, V) \\ H_{mu}(\omega, V) & H_{m\theta}(\omega, V) \end{bmatrix} \begin{bmatrix} \boldsymbol{\Phi}_j(z) & \boldsymbol{\Phi}_k(z) \end{bmatrix} dz \end{aligned} \quad (4.24)$$

$\mathbf{A}_a(\omega, V)$  fulfills the following symmetry properties

$$\left. \begin{aligned} \operatorname{Re}(\mathbf{A}_a(\omega, V)) &= \operatorname{Re}(\mathbf{A}_a(-\omega, V)) \\ \operatorname{Im}(\mathbf{A}_a(\omega, V)) &= -\operatorname{Im}(\mathbf{A}_a(-\omega, V)) \end{aligned} \right\} \quad (4.25)$$

### 4.3 Flutter

From Eq.(4.9), (4.13), (4.22) and (4.23) follows

$$\begin{aligned} \mathbf{A}_s(\omega) \cdot \mathbf{Q} = \mathbf{F}(\omega, V) = \mathbf{A}_a(\omega, V) \cdot \mathbf{Q} \Rightarrow \\ (\mathbf{A}_s(\omega) - \mathbf{A}_a(\omega, V)) \cdot \mathbf{Q} = \mathbf{0} \end{aligned} \quad (4.26)$$

where:

$$\mathbf{A}_s(\omega) = \begin{bmatrix} A_j(\omega) & 0 \\ 0 & A_k(\omega) \end{bmatrix} \quad (4.27)$$

where  $A_j(\omega)$  indicates the inverse of the modal frequency response function  $H_j(\omega)$ , given as

$$A_j(\omega) = m_j (\omega_j^2 - \omega^2 + 2 \cdot \zeta_j \omega_j \omega i) \quad (4.28)$$

Eq.(4.26) is a system of linear homogeneous equations. Non-trivial solution  $\mathbf{Q} \neq \mathbf{0}$ , corresponding to onset of flutter, requires that:

$$\det(\mathbf{A}_s(\omega) - \mathbf{A}_a(\omega, V)) = 0 \quad (4.29)$$

Eq.(4.29) must be fulfilled for both the real and imaginary part of the determinant. This provides two nonlinear coupled equations from which the critical wind speed  $V_c$  and the angular frequency  $\omega_c$  at onset of flutter may be determined.

The indicated theory is the correct approach based on a truncated modal analysis with two critical modes. It deviates from the approach in [9], which lacks any reference to 3D effects (the different bridge deck response along the bridge).

## 4.4 Reduction of system of equations

The eigenmodes are ordered corresponding to ascending values of the undamped eigenfrequency  $f_j$  (see Table 3.5). In the following, the index  $j$  indicates a symmetric bending mode, and the index  $k$  indicates a symmetric torsional mode.

$$\left. \begin{aligned} U_j(z) \neq 0 & \quad , \quad \Theta_j(z) \equiv 0 \\ U_k(z) \equiv 0 & \quad , \quad \Theta_k(z) \neq 0 \end{aligned} \right\} \quad (4.30)$$

The bending modes are normalized, so:

$$\max U_j(z) = 1 \quad (4.31)$$

Correspondingly, the torsional modes are normalized, so:

$$\max \Theta_j(z) = 1 \quad (4.32)$$

With the indicated normalization, the modal coordinate  $\mathbf{Q}_j(z)$  have dimension of length, and  $\mathbf{Q}_k(z)$  is non-dimensional.

Flutter is assumed to take place as a coupling between the first, the second or the third symmetric bending mode, corresponding to  $j = 1, 3, 5$ , and the first symmetric torsional mode, corresponding to  $k = 1$ . Due to symmetry properties of the involved eigenmodes, this fulfill the properties of Figure 3.3 to 3.6. Then, the modal masses become:

$$\left. \begin{aligned} m_j &= \int_0^L \mu \cdot U_j^2(z) dz = \mu \cdot L \cdot a_{jj} \\ m_k &= \int_0^L J \cdot \Theta_k^2(z) dz = J \cdot L \cdot a_{kk} \end{aligned} \right\} \quad (4.33)$$

where:

$$\left. \begin{aligned} a_{jj} &= \frac{1}{L} \int_0^L U_j^2(z) dz \\ a_{jk} &= \frac{1}{L} \int_0^L U_j(z) \cdot \Theta_k(z) dz \\ a_{kk} &= \frac{1}{L} \int_0^L \Theta_k^2(x) dx \end{aligned} \right\} \quad (4.34)$$

$a_{jj}$ ,  $a_{jk}$  and  $a_{kk}$  are non-dimensional quantities with values in the interval ]0, 1[.

The matrix function  $\mathbf{A}_a(\omega, V)$  may be calculated as

$$\mathbf{A}_a(\omega, V) = \int_0^L \begin{bmatrix} a(z, \omega, V) & b(z, \omega, V) \\ c(z, \omega, V) & d(z, \omega, V) \end{bmatrix} d\zeta \quad (4.35)$$

where:

$$\begin{bmatrix} a(z, \omega, V) & b(z, \omega, V) \\ c(z, \omega, V) & d(z, \omega, V) \end{bmatrix} = \begin{bmatrix} H_{pu}(\omega, V) \cdot U_j^2(z) & H_{p\theta}(\omega, V) \cdot U_j(z) \cdot \Theta_k(z) \\ H_{mu}(\omega, V) \cdot U_j(z) \cdot \Theta_k(z) & H_{m\theta}(\omega, V) \cdot \Theta_k^2(z) \end{bmatrix} \quad (4.36)$$

The aeroelastic frequency response functions can be defined as:

$$\left. \begin{aligned} H_{pu}(\omega, V) &= \frac{1}{2} \cdot \rho \cdot V^2 \cdot h_{pu}(\Omega, V) \\ H_{mu}(\omega, V) &= \frac{1}{2} \cdot \rho \cdot V^2 \cdot B \cdot h_{mu}(\Omega, V) \\ H_{p\theta}(\omega, V) &= \frac{1}{2} \cdot \rho \cdot V^2 \cdot B \cdot h_{p\theta}(\Omega, V) \\ H_{m\theta}(\omega, V) &= \frac{1}{2} \cdot \rho \cdot V^2 \cdot B^2 \cdot h_{m\theta}(\Omega, V) \end{aligned} \right\} \quad (4.37)$$

where  $\Omega$  indicates a non-dimensional reduced angular frequency given as:

$$\Omega = \frac{\omega \cdot B}{V} \quad (4.38)$$

$h_{pu}(\Omega, V)$ ,  $h_{mu}(\Omega, V)$ ,  $h_{p\theta}(\Omega, V)$  and  $h_{m\theta}(\Omega, V)$  are non-dimensional frequency and velocity dependent lift-and moment coefficients. For  $\Omega \rightarrow 0$ ,  $h_{p\theta}(0)$  and  $h_{m\theta}(0)$  indicates the quasi-static lift-and moment coefficients  $c_l$  and  $c_m$  from 2D aerodynamics. If the aerodynamic center is assumed to be placed at the quarter point from the leading edge, and the moment load is referred to the center of the profile, then  $c_m \simeq \frac{1}{4} \cdot c_l$  as follows from potential flow theory from thin plates ([3]).

Then, Eq.(4.35) may be written as:

$$\mathbf{A}_a(\omega, V) = \frac{1}{2} \cdot \rho \cdot V^2 \cdot L \cdot \begin{bmatrix} h_{pu}(\Omega, V) \cdot a_{jj} & B \cdot h_{p\theta}(\Omega, V) \cdot a_{jk} \\ B \cdot h_{mu}(\Omega, V) \cdot a_{jk} & B^2 \cdot h_{m\theta}(\Omega, V) \cdot a_{kk} \end{bmatrix} \quad (4.39)$$

Similarly,  $\mathbf{A}_s(\boldsymbol{\omega})$  may be written as:

$$\mathbf{A}_s(\boldsymbol{\omega}) = \frac{V^2 \cdot L}{B^2} \cdot \begin{bmatrix} \mu \cdot a_{jj} \cdot (\Omega^2 - \Omega_j^2 + 2 \cdot \zeta_j \cdot \Omega_j \cdot \Omega) & 0 \\ 0 & J \cdot a_{kk} \cdot (\Omega^2 - \Omega_k^2 + 2 \cdot \zeta_k \cdot \Omega_k \cdot \Omega) \end{bmatrix} \quad (4.40)$$

where:

$$\Omega_j = \Omega_j(V) = \frac{\boldsymbol{\omega}_j \cdot \mathbf{B}}{V} \quad , \quad \Omega_k = \Omega_k(V) = \frac{\boldsymbol{\omega}_k \cdot \mathbf{B}}{V} \quad (4.41)$$

The singularity condition on Eq.(4.29), can then be reduced to:

$$\det(\mathbf{a}_s(\Omega, V) - \mathbf{a}_a(\Omega, V)) = 0 \quad (4.42)$$

where

$$\mathbf{a}_s(\Omega, V) = \begin{bmatrix} \Omega^2 - \Omega_j^2(V) + 2 \cdot \zeta_j \cdot \Omega_j(V) \cdot \Omega \cdot i & 0 \\ 0 & \Omega^2 - \Omega_k^2(V) + 2 \cdot \zeta_k \cdot \Omega_k(V) \cdot \Omega \cdot i \end{bmatrix} \quad (4.43)$$

$$\mathbf{a}_a(\Omega, V) = \frac{1}{2} \cdot \rho \cdot B^2 \cdot \begin{bmatrix} \frac{1}{\mu} \cdot h_{pu}(\Omega, V) & \frac{B}{\mu} \cdot \frac{a_{jk}}{a_{jj}} \cdot h_{p\theta}(\Omega, V) \\ \frac{B}{J} \cdot \frac{a_{jk}}{a_{kk}} \cdot h_{mu}(\Omega, V) & \frac{B^2}{J} \cdot h_{m\theta}(\Omega, V) \end{bmatrix} \quad (4.44)$$

## EVALUATION OF AERODYNAMIC PARAMETERS

*The scope of this Chapter is to evaluate the aerodynamic parameters from the theory described in Chapter 4. For this purpose, two methods are used: CFD simulations done in STAR-CCM+ and numerical solutions using MatLab. A full scale model of the bridge girder, performed in STAR-CCM+, subjected to a harmonic varying vertical displacement and forced rotation, is used to obtain the frequency response functions. Further, the remaining aerodynamic parameters are evaluated numerically.*

### 5.1 Background in CFD

Due to the author's limited knowledge of CFD beforehand, some time was applied in research on the matter. Two main sources were chosen in order to gain confidence within the topic ([6] and [12]).

Regarding *STAR-CCM+*, the usage of this tool was completely new to the author. Tutorials presented on the user guide literature [2] were conducted, as well as, the cases done in [6]. The author considered confidence acquired when the results obtained matched the ones from the sources. Due to time limitations, some of the parameters subjected to sensitivity analysis as, domain and mesh size, are chosen from [6], based on the parameters the source authors considered as convergent.

## 5.2 Description of the CFD model

Following the drawings on Appendix A, a full scale cross section of the bridge girder has been modelled using the build-in CAD-designer tool. In order to maintain the model simple, however, with the necessary attention to details which may influence the fluid-body interaction, the girder is made including the lateral and central railings, but omitting the hangers, cables and other vertical standing components. Each parameter of the model is described in detail along the following subsections.

### 5.2.1 Inputs

The aeroelastic analysis is performed by the *STAR-CCM+* code. The input to the software must be in terms of harmonic varying velocities  $\dot{u}(t)$  in the  $y$  direction and angular velocities  $\dot{\theta}(t)$  in the  $z$  direction, i.e.:

$$\left. \begin{aligned} \dot{u}(t) &= \dot{u}_0 \cdot e^{i \cdot \omega \cdot t} \\ \dot{\theta}(t) &= \dot{\theta}_0 \cdot e^{i \cdot \omega \cdot t} \end{aligned} \right\} \quad (5.1)$$

Correspondingly, the obtained frequency response functions for the load per unit length  $p(t)$  and moment load per unit length  $m(t)$  on the bridge deck obtained from the software are denoted as  $H_{p\dot{u}}(\omega)$ ,  $H_{p\dot{\theta}}(\omega)$ ,  $H_{m\dot{u}}(\omega)$  and  $H_{m\dot{\theta}}(\omega)$ .

However, in the modal analysis the frequency response functions  $H_{pu}(\omega)$ ,  $H_{p\theta}(\omega)$ ,  $H_{mu}(\omega)$  and  $H_{m\theta}(\omega)$  as driven by the vertical displacement  $u(t)$  and the rotation  $\theta(t)$  are needed. A relation between these and the frequency response functions from the *STAR-CCM+* code is given in the following.

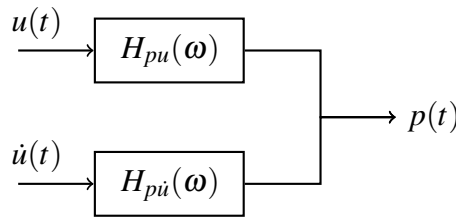


Fig. 5.1 Frequency response function for  $p(t)$  due to harmonic varying displacement and velocity of the bridge deck

The harmonic varying load per unit length is given as:

$$p(t) = p_0 \cdot e^{i \cdot \omega \cdot t} \quad (5.2)$$

where the complex amplitude  $p_0$  per definition becomes:

$$p_0 = H_{pu}(\omega) \cdot u_0 = H_{p\dot{u}}(\omega) \cdot \dot{u}_0 \quad (5.3)$$

Now,  $\dot{u}_0 = i \cdot \omega \cdot u_0$ . Hence, Eq.(5.3) provides the relation:

$$H_{pu}(\omega) = i \cdot \omega \cdot H_{p\dot{u}}(\omega) = e^{i \cdot \frac{\pi}{2}} \cdot \omega \cdot H_{p\dot{u}}(\omega) \quad (5.4)$$

$H_{p\dot{u}}(\omega)$  may be written on the polar form:

$$H_{p\dot{u}}(\omega) = |H_{p\dot{u}}(\omega)| \cdot e^{-i \cdot \phi_{p\dot{u}}(\omega)} \quad (5.5)$$

where  $\phi_{p\dot{u}}(\omega)$  indicates the phase lag of  $p(t)$  relative to  $\dot{u}(t)$ .

Similarly,  $H_{pu}(\omega)$  may be written as:

$$\begin{aligned} H_{pu}(\omega) &= |H_{pu}(\omega)| \cdot e^{-i \cdot \phi_{pu}(\omega)} \\ &= \omega \cdot |H_{p\dot{u}}(\omega)| \cdot e^{-i \cdot (\phi_{p\dot{u}}(\omega) - \frac{\pi}{2})} \end{aligned} \quad (5.6)$$

Hence, the modulus  $|H_{pu}(\omega)|$  and phase lag  $\phi_{pu}(\omega)$  of  $p(t)$  relative to  $u(t)$  are given as:

$$|H_{pu}(\omega)| = \omega \cdot |H_{p\dot{u}}(\omega)| \quad , \quad \phi_{pu}(\omega) = \phi_{p\dot{u}}(\omega) - \frac{\pi}{2} \quad (5.7)$$

Similarly, moduli and phase lags of the frequency response functions  $H_{p\theta}(\omega)$ ,  $H_{mu}(\omega)$  and  $H_{m\theta}(\omega)$  are given as:

$$\left. \begin{aligned} |H_{p\theta}(\omega)| &= \omega \cdot |H_{p\dot{\theta}}(\omega)| \quad , \quad \phi_{p\theta}(\omega) = \phi_{p\dot{\theta}}(\omega) - \frac{\pi}{2} \\ |H_{mu}(\omega)| &= \omega \cdot |H_{m\dot{u}}(\omega)| \quad , \quad \phi_{mu}(\omega) = \phi_{m\dot{u}}(\omega) - \frac{\pi}{2} \\ |H_{m\theta}(\omega)| &= \omega \cdot |H_{m\dot{\theta}}(\omega)| \quad , \quad \phi_{m\theta}(\omega) = \phi_{m\dot{\theta}}(\omega) - \frac{\pi}{2} \end{aligned} \right\} \quad (5.8)$$

Finally,  $h_{pu}(\omega, V)$ ,  $h_{p\theta}(\omega, V)$ ,  $h_{mu}(\omega, V)$  and  $h_{m\theta}(\omega, V)$  follow from Eq.(4.37).

## 5.2.2 Domain size

In order to perform a CFD simulation, a domain must be defined. The size of the domain should be as large as the edges of it do not influence or limit the flow. However, large domain containing a refined mesh can end up in a large simulation time. In order to find the balance

between accuracy and simulation time, a smaller domain is created just around the bridge girder with refined mesh. The dimensions of the main domain are shown in Figure 5.2. As state in Section 5.1, the dimensions considered are based on [6].

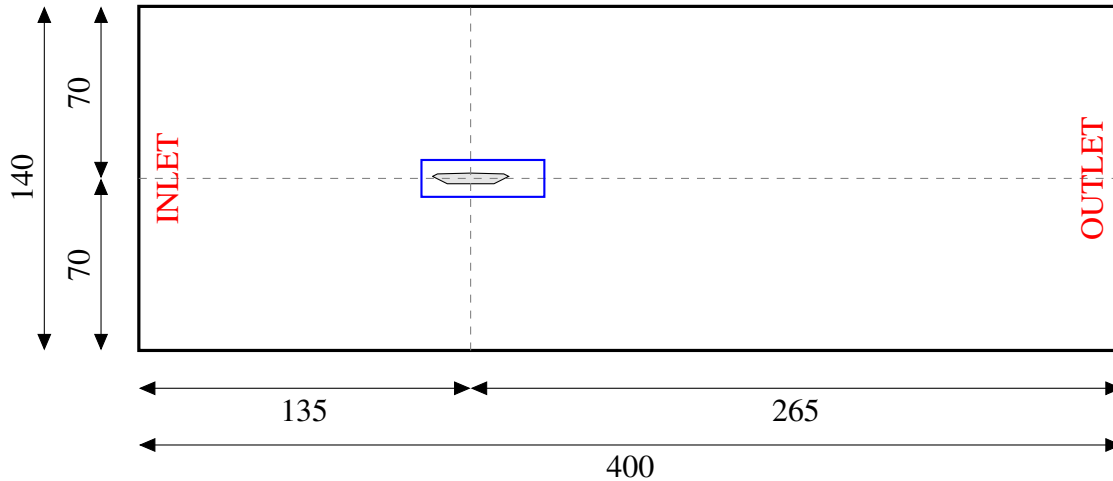


Fig. 5.2 Main domain size  
(dimensions in m)

For the girder domain (marked in blue in Figure 5.2), 50x15m size is adopted, vertically centred and with 20m to the inlet side and 30m in the opposite direction. The area towards the inlet is considered sufficiently large to avoid interference of the uniform incoming flow, and the opposite area, towards the outlet, sufficiently large to observe wakes and its vanishing.

### 5.2.3 Mesh size

The mesh size plays an important role in any numerical model. However, one should be aware that the meshing process needs to account for the aim of the simulation, meaning that not the entire domain required a fine mesh. In *STAR-CCM+* the process is done using an automated built-in tool which allows the user to define the base mesh (the coarser mesh) for the areas with low or none variation, and the customized refined mesh based on a percentage of the base mesh parameters, for the areas where the flow motion is of interest.

In Figure 5.3, the different mesh setups can be seen, and are as follows:

1. Domain mesh: represents the coarse mesh applied in most of the domain;
2. Girder mesh: a refined mesh around the bridge girder, in order to obtain an accurate flow observation;
3. Wake refinement: as the name indicate, a finer mesh is applied in the wake zone;

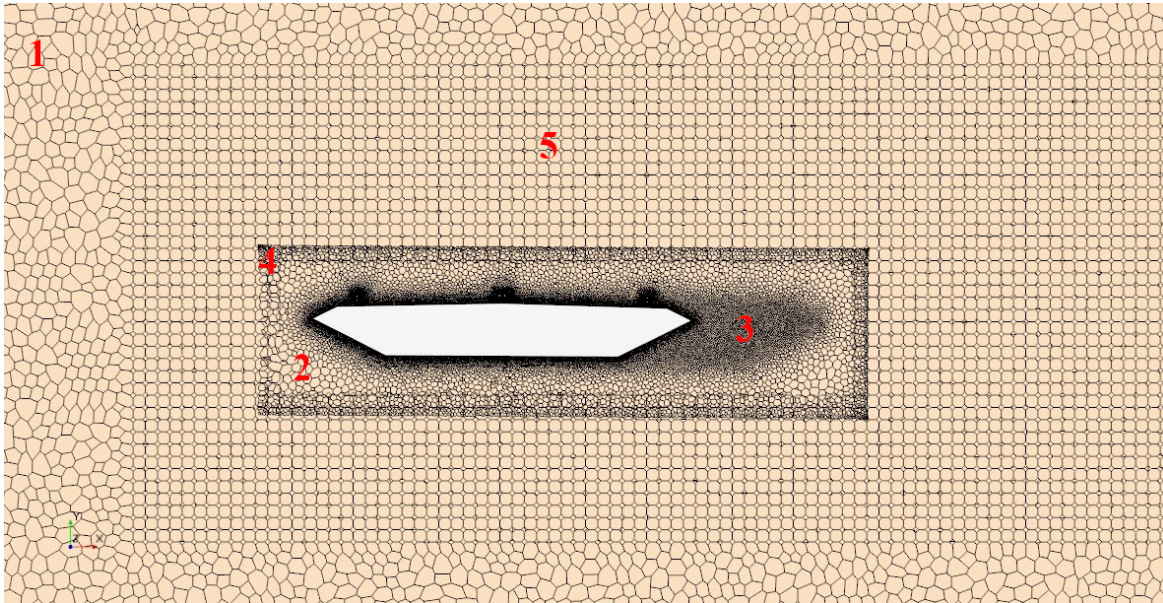


Fig. 5.3 Mesh domains and refinements

4. Overset mesh interface: this is a built-in tool from *STAR-CCM+* which allow the connection between the domain mesh and the girder mesh. This is needed due to the moving condition of the girder since the girder mesh will change in every time step of the motion;
5. Volumetric mesh: the purpose of this area is to make a smooth transition between the coarse and fine mesh. A volumetric control is therefore applied by inserting the values of size mesh for both, coarse and fine areas.

Beside the different mesh setups, surface controls are applied in the girder and railing, and curve controls applied along the edges of the girder.

A resume of the mesh parameters is shown in Table 5.1.

Table 5.1 Mesh input parameters

<b>Domain mesh</b>	Input	Unit
Base size	3	[m]
Surface growth rate	1.3	[-]
<b>Volumetric control</b>		
Custom size	33.33	[%]
<b>Girder mesh</b>		
Base size	1	[m]
Surface growth rate	1.2	[-]
<b>Surface control - girder</b>		
Surface size	5	[%]
Surface growth rate	1.1	[-]
Wake size	12.5	[%]
Wake range	10	[m]
Wake growth rate	1.3	[-]
<b>Surface control - railing</b>		
Surface size	5	[%]
Surface growth rate	1.1	[-]
Wake size	5	[%]
Wake range	0.5	[m]
Wake growth rate	1.3	[-]
Wake spread angle	0.1	[rad]
<b>Curve controls - girder</b>		
Surface size	1	[%]

#### 5.2.4 Physics and solver

For the purpose of investigate air flow, the material is set to be gas with a constant density,  $\rho$  equal to  $1.225 \frac{\text{kg}}{\text{m}^3}$  and the kinematic viscosity  $\nu$  equal to  $1.48 \cdot 10^{-5} \frac{\text{m}^2}{\text{s}}$ . A turbulent viscous regime has been chosen and the turbulence model set to SST k- $\omega$ .

At the initial phase of the simulation, the response is influenced by the initial value of the response quantities. The following plots refer to a state where a stationary periodic response under the harmonic excitation is achieved.

### 5.3 Response functions

The CFD simulation is conducted for a translational motion  $u(t)$  with amplitude  $\dot{u}_0$  of  $0.4 \frac{\text{m}}{\text{s}}$ , and a rotational motion  $\theta(t)$  with amplitude  $\dot{\theta}_0$  of  $0.028 \frac{\text{rad}}{\text{s}}$ . These are considered sufficient small, that the responses in terms of the load and moment load per unit length become linear functions of  $u(t)$  and  $\theta(t)$ .

In both cases, the flow is assumed to be uniform in the total height of the incoming flow and the velocity  $V$ , set to be equal to  $50 \frac{\text{m}}{\text{s}}$  corresponding to  $Re = 1.04 \cdot 10^8$ , and the frequency of excitation is defined as 0.128Hz. The parameters above corresponds to the non-dimensional angular frequency  $\Omega$  equal to 0.5, cf. Eq.(4.38).

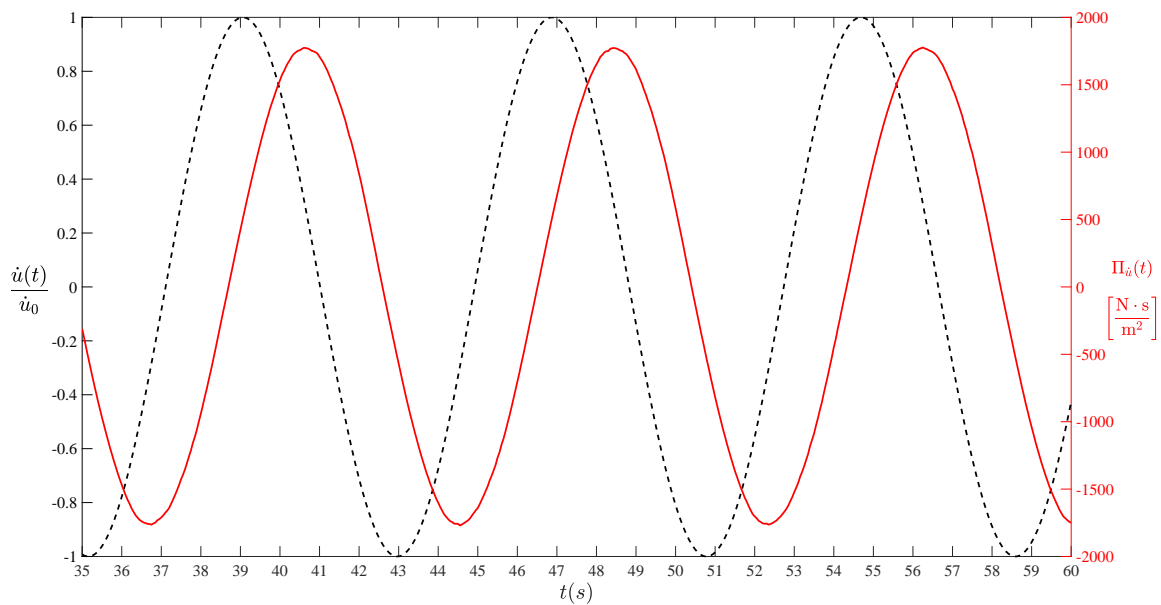


Fig. 5.4 Time series for the normalized and centralized load per unit length due to a harmonic varying vertical velocity of the bridge deck

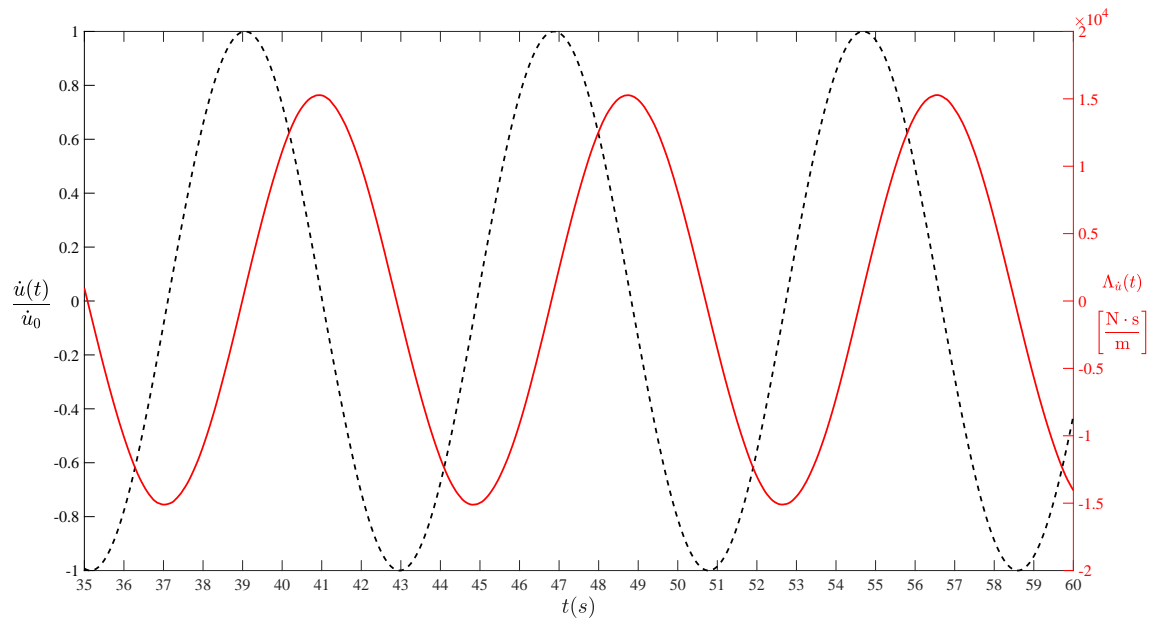


Fig. 5.5 Time series for the normalized and centralized moment load per unit length due to a harmonic varying velocity displacement of the bridge deck

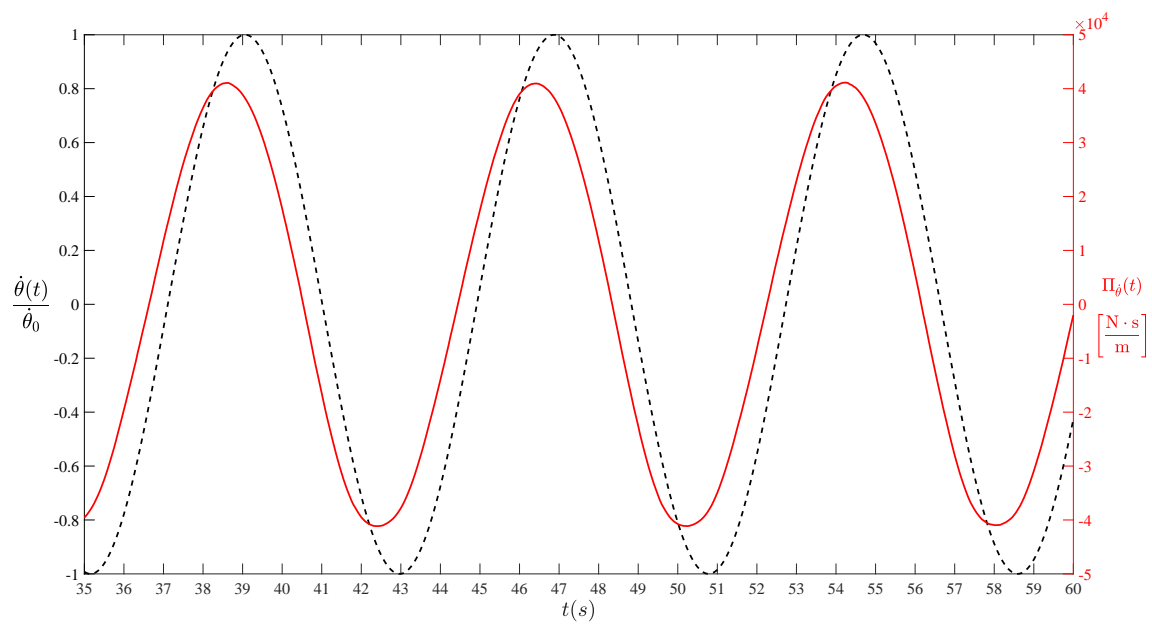


Fig. 5.6 Time series for the normalized and centralized load per unit length due to a harmonic varying angular velocity of the bridge deck

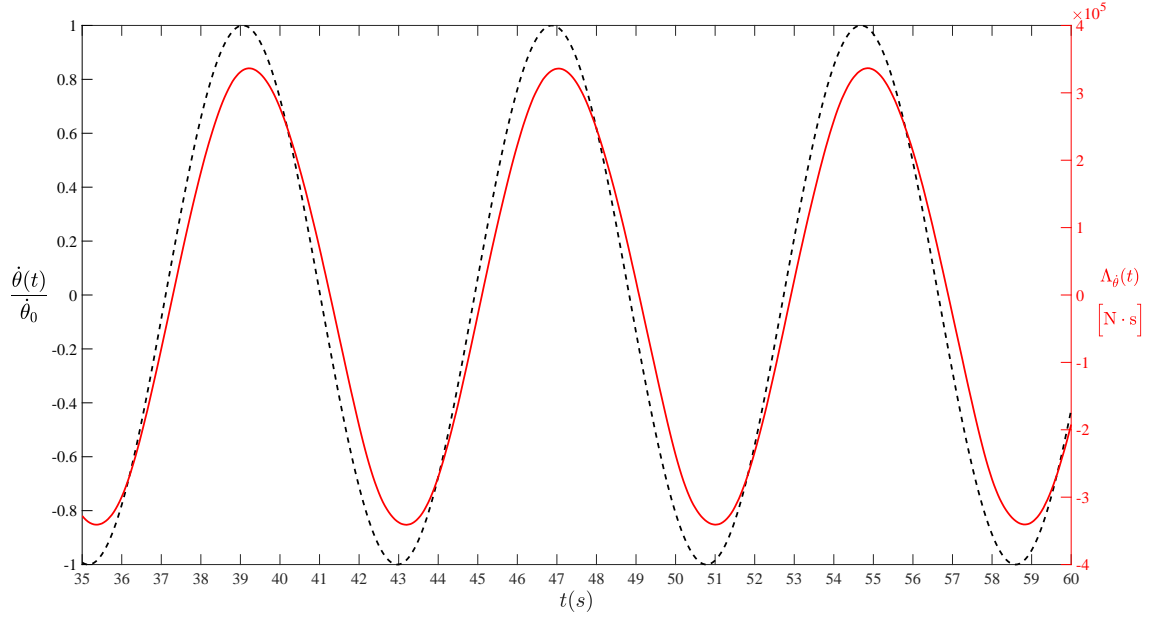


Fig. 5.7 Time series for the normalized and centralized moment load per unit length due to a harmonic varying angular velocity of the bridge deck

The non-dimensional quantities  $\Pi_{\dot{u}}(t)$ ,  $\Pi_{\dot{\theta}}(t)$ ,  $\Lambda_{\dot{u}}(t)$  and  $\Lambda_{\dot{\theta}}(t)$  are defined as:

$$\left. \begin{aligned} \Pi_{\dot{u}}(t) &= \frac{p(t) - \bar{p}}{\dot{u}_0} & , & \quad \Pi_{\dot{\theta}}(t) = \frac{p(t) - \bar{p}}{\dot{\theta}_0} \\ \Lambda_{\dot{u}}(t) &= \frac{m(t) - \bar{m}}{\dot{u}_0} & , & \quad \Lambda_{\dot{\theta}}(t) = \frac{m(t) - \bar{m}}{\dot{\theta}_0} \end{aligned} \right\} \quad (5.9)$$

where  $\bar{p}$  and  $\bar{m}$  represent time averages of the related  $p(t)$  and  $m(t)$  caused by either  $\dot{u}(t)$  or  $\dot{\theta}(t)$  defined as:

$$\bar{p} = \frac{1}{T} \cdot \int_0^T p(t) dt \quad , \quad \bar{m} = \frac{1}{T} \cdot \int_0^T m(t) dt \quad (5.10)$$

$T$  indicates the period of the harmonic excitations.

The phase lag  $\phi$  of a function with the time variation  $\cos(\omega \cdot t - \phi)$  caused by the harmonic variation  $\cos(\omega \cdot t)$  is determined from the relation:

$$\cos(\phi) = \frac{2}{T} \cdot \int_0^T \cos(\omega \cdot t - \phi) \cdot \cos(\omega \cdot t) dt \quad (5.11)$$

Assuming that  $\Pi_{\dot{u}}(t)$ ,  $\Lambda_{\dot{u}}(t)$ ,  $\Pi_{\dot{\theta}}(t)$  and  $\Lambda_{\dot{\theta}}(t)$  are harmonic varying and with the period  $T$  and the amplitudes  $|H_{p\dot{u}}(\Omega, V)|$ ,  $|H_{p\dot{\theta}}(\Omega, V)|$ ,  $|H_{m\dot{u}}(\Omega, V)|$  and  $|H_{m\dot{\theta}}(\Omega, V)|$ , the related phase lags  $\phi_{p\dot{u}}$ ,  $\phi_{m\dot{u}}$ ,  $\phi_{p\dot{\theta}}$  and  $\phi_{m\dot{\theta}}$  are calculated from:

$$\left. \begin{aligned} \cos(\phi_{p\dot{u}}) &= \frac{2}{T} \cdot \frac{\int_0^T \Pi_{\dot{u}}(t) \cdot \cos(\omega \cdot t) dt}{|H_{p\dot{u}}(\Omega, V)|} , & \cos(\phi_{p\dot{\theta}}) &= \frac{2}{T} \cdot \frac{\int_0^T \Pi_{\dot{\theta}}(t) \cdot \cos(\omega \cdot t) dt}{|H_{p\dot{\theta}}(\Omega, V)|} \\ \cos(\phi_{m\dot{u}}) &= \frac{2}{T} \cdot \frac{\int_0^T \Lambda_{\dot{u}}(t) \cdot \cos(\omega \cdot t) dt}{|H_{m\dot{u}}(\Omega, V)|} , & \cos(\phi_{m\dot{\theta}}) &= \frac{2}{T} \cdot \frac{\int_0^T \Lambda_{\dot{\theta}}(t) \cdot \cos(\omega \cdot t) dt}{|H_{m\dot{\theta}}(\Omega, V)|} \end{aligned} \right\} \quad (5.12)$$

where

$$\left. \begin{aligned} |H_{p\dot{u}}(\Omega, V)| &= \sqrt{2} \cdot \sqrt{\frac{1}{T} \cdot \int_0^T \Pi_{\dot{u}}^2(t) dt} , & |H_{p\dot{\theta}}(\Omega, V)| &= \sqrt{2} \cdot \sqrt{\frac{1}{T} \cdot \int_0^T \Pi_{\dot{\theta}}^2(t) dt} \\ |H_{m\dot{u}}(\Omega, V)| &= \sqrt{2} \cdot \sqrt{\frac{1}{T} \cdot \int_0^T \Lambda_{\dot{u}}^2(t) dt} , & |H_{m\dot{\theta}}(\Omega, V)| &= \sqrt{2} \cdot \sqrt{\frac{1}{T} \cdot \int_0^T \Lambda_{\dot{\theta}}^2(t) dt} \end{aligned} \right\} \quad (5.13)$$

The dimensions of  $|H_{p\dot{u}}(\Omega, V)|$ ,  $|H_{p\dot{\theta}}(\Omega, V)|$ ,  $|H_{m\dot{u}}(\Omega, V)|$  and  $|H_{m\dot{\theta}}(\Omega, V)|$  are, respectively,  $\left[ \frac{\text{N} \cdot \text{s}}{\text{m}^2} \right]$ ,  $\left[ \frac{\text{N} \cdot \text{s}}{\text{m}} \right]$ ,  $\left[ \frac{\text{N} \cdot \text{s}}{\text{m}} \right]$  and  $[\text{N} \cdot \text{s}]$ .

Eq.(5.12) is evaluated numerically and the results are as follow on Table 5.2.

Table 5.2 Phase lag  $\phi$

Phase lag	Value [rad]
$\phi_{p\dot{u}}$	1.275
$\phi_{m\dot{u}}$	1.510
$\phi_{p\dot{\theta}}$	-0.400
$\phi_{m\dot{\theta}}$	0.174

Then, the frequency response functions  $H_{p\dot{u}}(\Omega, V)$ ,  $H_{m\dot{u}}(\Omega, V)$ ,  $H_{p\dot{\theta}}(\Omega, V)$  and  $H_{m\dot{\theta}}(\Omega, V)$  are given as:

$$\left. \begin{aligned} H_{p\dot{u}}(\Omega, V) &= |H_{p\dot{u}}(\Omega, V)| \cdot (\cos \phi_{p\dot{u}} - i \cdot \sin \phi_{p\dot{u}}) \\ H_{m\dot{u}}(\Omega, V) &= |H_{m\dot{u}}(\Omega, V)| \cdot (\cos \phi_{m\dot{u}} - i \cdot \sin \phi_{m\dot{u}}) \\ H_{p\dot{\theta}}(\Omega, V) &= |H_{p\dot{\theta}}(\Omega, V)| \cdot (\cos \phi_{p\dot{\theta}} - i \cdot \sin \phi_{p\dot{\theta}}) \\ H_{m\dot{\theta}}(\Omega, V) &= |H_{m\dot{\theta}}(\Omega, V)| \cdot (\cos \phi_{m\dot{\theta}} - i \cdot \sin \phi_{m\dot{\theta}}) \end{aligned} \right\} \quad (5.14)$$

## 5.4 Evaluation of $\Omega_c$ and $V_c$

From Eq.(4.42) let  $\mathbf{A}(\Omega, V) = \mathbf{a}_s(\Omega, V) - \mathbf{a}_a(\Omega, V)$ . The critical wind velocity  $V_c$  and related non-dimensional reduced angular frequency  $\Omega_c$  are determined from:

$$\begin{aligned} \det(\mathbf{A}) &= A_{11} \cdot A_{22} - A_{12} \cdot A_{21} \\ &= f_1(\Omega_c, V_c) + i \cdot f_2(\Omega_c, V_c) = 0 \end{aligned} \quad (5.15)$$

where:

$$\left. \begin{aligned} f_1(\Omega_c, V_c) &= \text{Re}(A_{11}) \cdot \text{Re}(A_{22}) - \text{Im}(A_{11}) \cdot \text{Im}(A_{22}) \\ &\quad - \text{Re}(A_{12}) \cdot \text{Re}(A_{21}) + \text{Im}(A_{12}) \cdot \text{Im}(A_{21}) \\ f_2(\Omega_c, V_c) &= \text{Re}(A_{11}) \cdot \text{Im}(A_{22}) + \text{Im}(A_{11}) \cdot \text{Re}(A_{22}) \\ &\quad - \text{Re}(A_{12}) \cdot \text{Im}(A_{21}) - \text{Im}(A_{12}) \cdot \text{Re}(A_{21}) \end{aligned} \right\} \quad (5.16)$$

Further, let:

$$\mathbf{x} = \begin{bmatrix} \Omega_c \\ V_c \end{bmatrix}, \quad \mathbf{f}(\Omega_c, V_c) = \begin{bmatrix} f_1(\Omega_c, V_c) \\ f_2(\Omega_c, V_c) \end{bmatrix} \quad (5.17)$$

Then Eq.(5.15) may be written as:

$$\mathbf{f}(\mathbf{x}) = \mathbf{0} \quad (5.18)$$

### Newton-Raphson iteration

Given a present iterated solution  $\mathbf{x}_0$ , so  $\mathbf{f}(\mathbf{x}_0) \neq \mathbf{0}$ . Determine a new solution  $\mathbf{x}_1 = \mathbf{x}_0 + \Delta \mathbf{x}$ , so:

$$\mathbf{f}(\mathbf{x}_0 + \Delta \mathbf{x}) = \mathbf{0} \quad (5.19)$$

First order Taylor expansion of Eq.(5.19) provides the following solution for  $\mathbf{x}_1$ :

$$\begin{aligned} \mathbf{f}(\mathbf{x}_0) + \nabla\mathbf{f}(\mathbf{x}_0) \cdot \Delta\mathbf{x} &\Rightarrow \\ \mathbf{x}_1 = \mathbf{x}_0 + \Delta\mathbf{x} = \mathbf{x}_0 - (\nabla\mathbf{f}(\mathbf{x}_0))^{-1} \cdot \mathbf{f}(\mathbf{x}_0) &\quad (5.20) \end{aligned}$$

where the gradient of  $\mathbf{f}(\mathbf{x}_0)$  is given as:

$$\nabla\mathbf{f}(\mathbf{x}) = \begin{bmatrix} \frac{\partial f_1}{\partial \Omega} & \frac{\partial f_1}{\partial V} \\ \frac{\partial f_2}{\partial \Omega} & \frac{\partial f_2}{\partial V} \end{bmatrix} \quad (5.21)$$

The partial derivatives in Eq.(5.21) are evaluated numerically.

## 5.5 Dependency of the frequency response function on $\omega$ and $V$

It is currently assumed by bridge design offices, that the flutter derivatives do not depend on Reynolds number, thus independent of the mean wind velocity  $V$ . In the present context, this means that the frequency response functions  $H_{pu}(\Omega, V)$ ,  $H_{mu}(\Omega, V)$ ,  $H_{p\theta}(\Omega, V)$  and  $H_{m\theta}(\Omega, V)$  should also be independent of  $V$ . This hypothesis will be investigated in the present Section.

The methodology will be to investigate the load response to harmonic varying velocities  $\dot{u}(t)$  in the  $y$  direction and angular velocities  $\dot{\theta}(t)$  in the  $z$  direction with the angular frequencies  $\omega = 0.4 \frac{\text{rad}}{\text{s}}$  and  $\omega = 0.8 \frac{\text{rad}}{\text{s}}$ , respectively. The related mean wind velocities are chosen as  $V = 25 \frac{\text{rad}}{\text{s}}$  and  $V = 50 \frac{\text{rad}}{\text{s}}$ , so the fraction  $\frac{\omega}{V}$  is constant. The amplitudes  $\dot{u}_0$  and  $\dot{\theta}_0$  of the excitations are unchanged in the two investigations.

Then, if the frequency response functions  $H_{p\dot{u}}(\Omega, V)$ ,  $H_{m\dot{u}}(\Omega, V)$ ,  $H_{p\dot{\theta}}(\Omega, V)$  and  $H_{m\dot{\theta}}(\Omega, V)$  are essential identical in the two investigations, it may be concluded that the mentioned frequency response functions merely depend on  $\omega$  and  $V$  via the non-dimensional frequency  $\Omega = \frac{\omega \cdot B}{V}$  in the indicated ranges of  $\omega$  and  $V$ , and hence is independent of the Reynolds number.

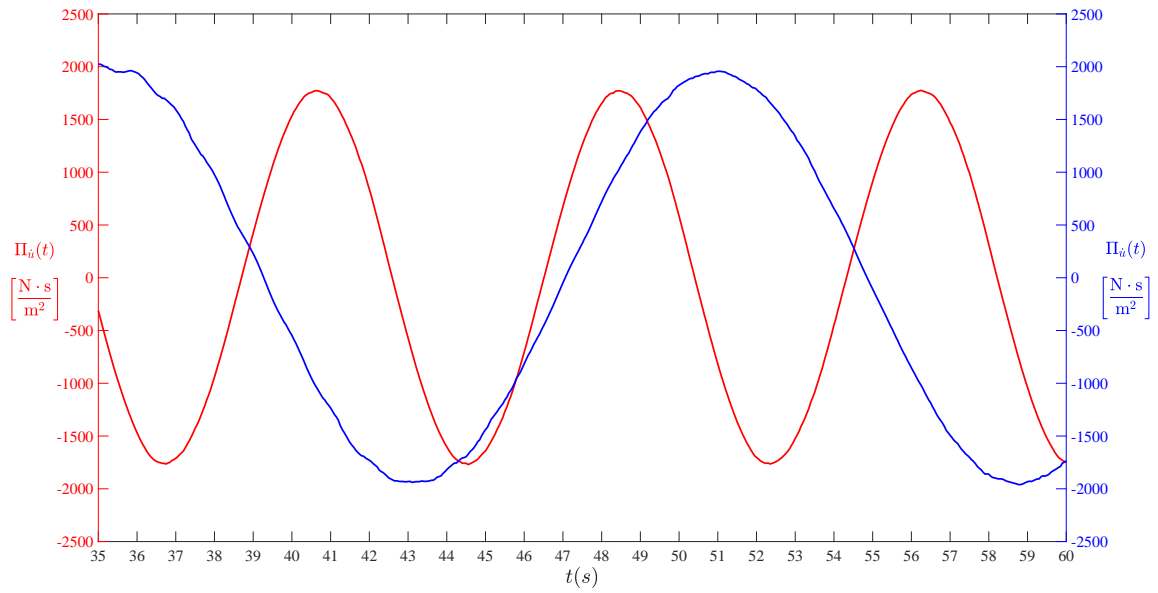


Fig. 5.8 Variation of  $\Pi_{ii}(t)$ ; Red curve,  $\omega = 0.8 \frac{\text{rad}}{\text{s}}$ , Blue curve,  $\omega = 0.4 \frac{\text{rad}}{\text{s}}$

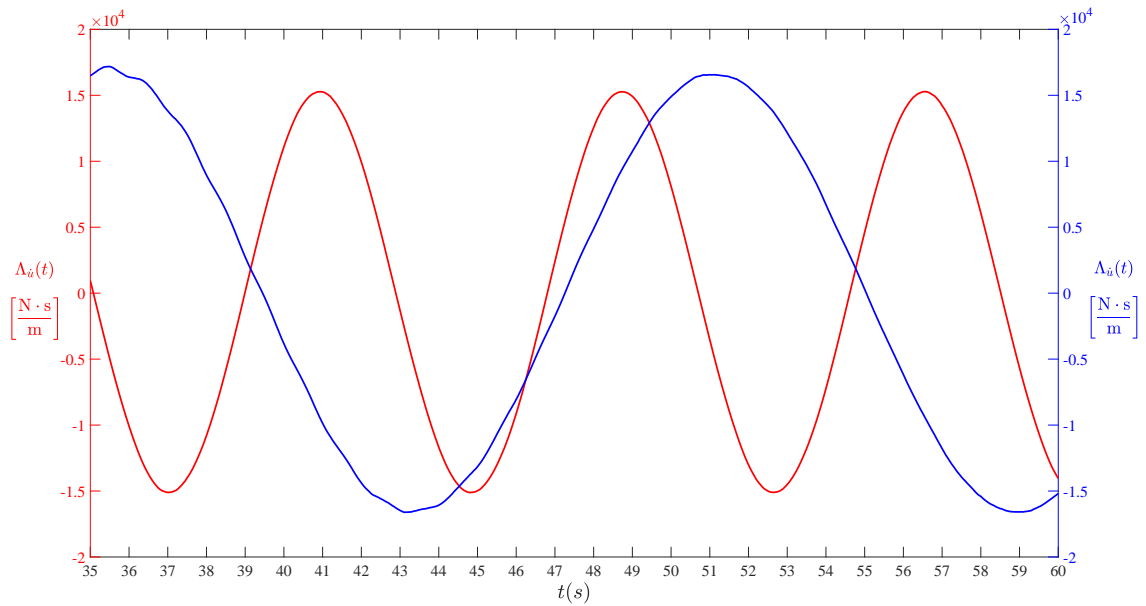


Fig. 5.9 Variation of  $\Lambda_{ii}(t)$ ; Red curve,  $\omega = 0.8 \frac{\text{rad}}{\text{s}}$ , Blue curve,  $\omega = 0.4 \frac{\text{rad}}{\text{s}}$

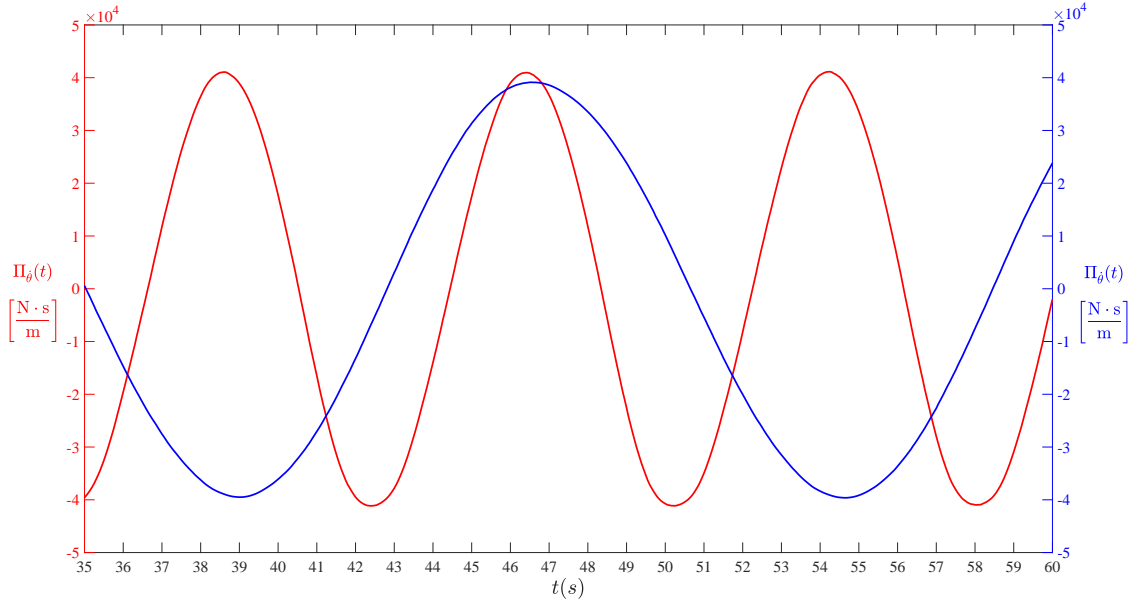


Fig. 5.10 Variation of  $\Pi_{\theta}(t)$ ; Red curve,  $\omega = 0.8 \frac{\text{rad}}{\text{s}}$ , Blue curve,  $\omega = 0.4 \frac{\text{rad}}{\text{s}}$

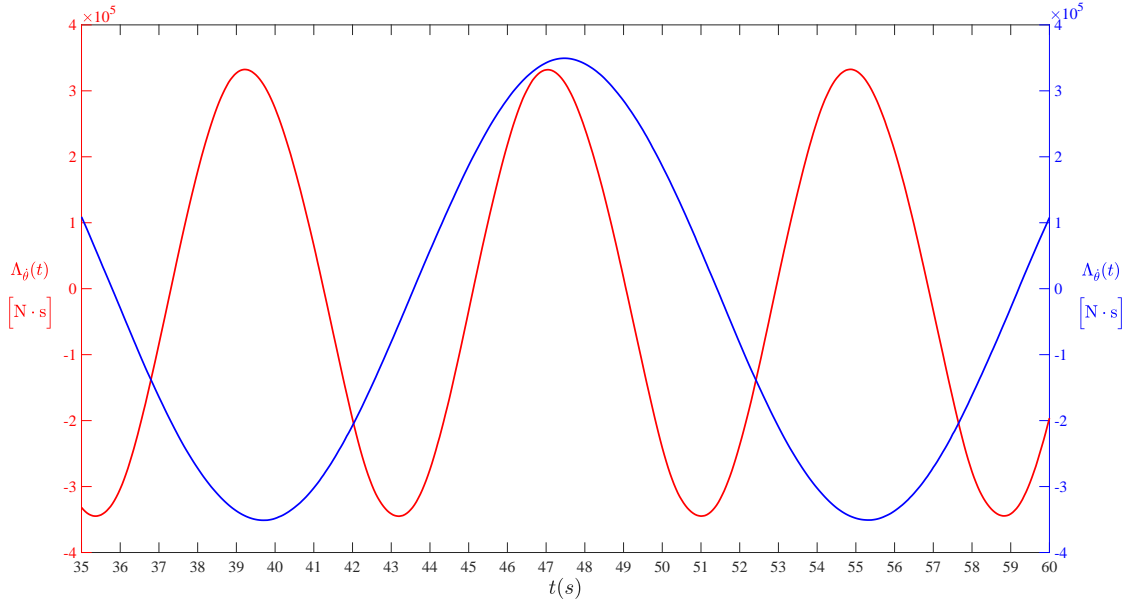


Fig. 5.11 Variation of  $\Lambda_{\theta}(t)$ ; Red curve,  $\omega = 0.8 \frac{\text{rad}}{\text{s}}$ , Blue curve,  $\omega = 0.4 \frac{\text{rad}}{\text{s}}$

Figures 5.8 to 5.11 illustrate the normalized and centralized loads per unit length  $\Pi_{\dot{u}}(t)$ ,  $\Pi_{\dot{\theta}}(t)$ , and the normalized and centralized moment loads per unit length  $\Lambda_{\dot{u}}(t)$ ,  $\Lambda_{\dot{\theta}}(t)$  for angular frequencies of  $0.8 \frac{\text{rad}}{\text{s}}$  and  $0.4 \frac{\text{rad}}{\text{s}}$  respectively. Based on the relations in Eq.(5.12) and Eq.(5.13) the following amplitudes  $|H_{p\dot{u}}(\Omega, V)|$ ,  $|H_{p\dot{\theta}}(\Omega, V)|$ ,  $|H_{m\dot{u}}(\Omega, V)|$ ,  $|H_{m\dot{\theta}}(\Omega, V)|$  and phase lags  $\phi_{p\dot{u}}$ ,  $\phi_{m\dot{u}}$ ,  $\phi_{p\dot{\theta}}$  and  $\phi_{m\dot{\theta}}$  are obtained:

Table 5.3 Frequency response functions and phase lags

	$\omega = 0.4 \frac{\text{rad}}{\text{s}}$ $V = 25 \frac{\text{m}}{\text{s}}$	$\omega = 0.8 \frac{\text{rad}}{\text{s}}$ $V = 50 \frac{\text{m}}{\text{s}}$	Variation [%]
$ H_{p\dot{u}}  \left[ \frac{\text{N} \cdot \text{s}}{\text{m}^2} \right]$	$1.95 \cdot 10^3$	$1.77 \cdot 10^3$	9.2
$ H_{m\dot{u}}  \left[ \frac{\text{N} \cdot \text{s}}{\text{m}} \right]$	$1.66 \cdot 10^4$	$1.52 \cdot 10^4$	8.4
$ H_{p\dot{\theta}}  \left[ \frac{\text{N} \cdot \text{s}}{\text{m}} \right]$	$3.95 \cdot 10^4$	$4.16 \cdot 10^4$	-5.3
$ H_{m\dot{\theta}}  \left[ \text{N} \cdot \text{s} \right]$	$3.49 \cdot 10^5$	$3.39 \cdot 10^5$	2.9
$\phi_{p\dot{u}}$ [rad]	1.645	1.275	22.5
$\phi_{m\dot{u}}$ [rad]	1.717	1.510	12.1
$\phi_{p\dot{\theta}}$ [rad]	-0.073	-0.400	-
$\phi_{m\dot{\theta}}$ [rad]	0.253	0.174	31.2

The variation in the third column of Table 5.3 is determined using the results in the first column as a reference.

As seen, the variations of the amplitudes are within 10%, whereas the variations on the phase lags are significantly larger. The inevitable conclusion seems to be that the obtained frequency response functions for the load and moment load per unit length does not merely depend on  $V$  and  $\omega$  via the reduced frequency  $\Omega = \frac{\omega \cdot B}{V}$ , as assumed in the classical flutter analysis based on the flutter derivatives.

After determining  $H_{p\dot{u}}(\omega, V)$ ,  $H_{m\dot{u}}(\omega, V)$ ,  $H_{p\dot{\theta}}(\omega, V)$  and  $H_{m\dot{\theta}}(\omega, V)$ , the related frequency functions  $H_{pu}(\omega, V)$ ,  $H_{p\theta}(\omega, V)$ ,  $H_{mu}(\omega, V)$  and  $H_{m\theta}(\omega, V)$  are determined from Eq.(5.8).

Next, the normalized frequency response functions  $h_{pu}(\Omega, V)$ ,  $h_{p\theta}(\Omega, V)$ ,  $h_{mu}(\Omega, V)$  and  $h_{m\theta}(\Omega, V)$  are obtained from Eq.(4.37), and the matrices  $\mathbf{a}_s(\Omega, V)$  and  $\mathbf{a}_a(\Omega, V)$  from Eq.(4.43) and Eq.(4.44).

Finally, the functions  $f_1(\Omega, V)$  and  $f_2(\Omega, V)$  are calculated by means of Eq.(5.15) Eq.(5.16).



## CONCLUSION

Due to the current highly use of computational resources, the approach taken into account along this thesis represent an improvement in obtaining the frequency response by means of CFD. This method reflects a significant decrease in time and cost, since wind tunnel tests has an high cost and require significant time for setting up the simulations. Beside that, the use of CFD allows to reach supercritical Reynolds number, whereas only subcritical levels can be achieved in the model testing. Although in wind tunnel testing is possible to simulate full scale models, this highly influence the costs of the procedure. When down-scaling the models, errors can occur. None of mentioned considerations exist while using CFD, since the time of simulations merely depends on the computational power available.

With the procedure mentioned in Section 5.5, the critical values for onset of flutter can be evaluated. Due to the lack of time, this step is left for further framework. It is suggested to perform a tabulation of the real and imaginary parts of the normalized frequency response functions  $h_{pu}(\Omega, V)$ ,  $h_{p\theta}(\Omega, V)$ ,  $h_{mu}(\Omega, V)$  and  $h_{m\theta}(\Omega, V)$  for the load per unit length  $p(t)$  and the moment load per unit length  $m(t)$ . Next, results of interest for different values of  $\Omega$  and  $V$  can be obtained by means of interpolation.

In the thesis the often applied hypothesis used in aeroelastic bridge engineering bridge engineering, that the so-called flutter derivatives are independent of Reynolds number and merely depends on the critical wind velocity and critical flutter angular frequency via a non-dimensional reduced frequency parameter. The flutter derivatives merely represent the real and imaginary parts of the frequency response functions for the loads and moment loads.

However, the CFD calculations, which are carried out for wind velocities of  $V = 25 \frac{\text{rad}}{\text{s}}$  and  $V = 50 \frac{\text{rad}}{\text{s}}$ , seems to question this assumption.

As proposal for future framework, it is recommended as follows:

- Up-scaling models: the up-scaling considerations from Section 1.5 should be verified or, in alternative, modified for the parameters close or equal to real bridge projects;
- Structural dynamic model: although the obtained values for eigenfrequencies are within an acceptable difference from the ones considered as reference values (see Table 3.4 and 3.5) it is of interest to validate against other sources and/or modify the current model in order to reach higher accuracy;
- CFD simulations: as mentioned in Section 5.1, the author had limited knowledge of CFD and no knowledge of the software *STAR-CCM+* beforehand. Although the author assumed to have reached sufficient confidence within the two topics, it is of interest to re-evaluate the modelling procedures and set up parameters considered, i.e., sensitivity analysis on the mesh size, time step and simulation time.

Based on the above described, the author assumes that the present thesis reached the initial aim, however, it has sufficient content to be subject of future frameworks, either to perform the proposed improvements, or to finalize the theory with a complete tabulation of the results of interest. This includes the determination of the critical flutter velocity  $V_c$  as a function of the main span  $L$ .

Finally, the author concludes that the combination of computational resources as *ABAQUS*, *STAR-CCM+* and *MatLab* or any other equivalent software, it represents an efficient and sufficiently accurate way to perform aerodynamic analysis, when compared to analytical, empirical and experimental methods used during the past decades.

## BIBLIOGRAPHY

- [1] Brincker, R; Frandsen, J. B. A. P. (2000). Ambient response analysis of the great belt bridge. *Proceedings of the International Modal Analysis Conference*.
- [2] CD-Adapco (2018). *STAR-CCM+ User Guide*. Germany: CD-Adapco.
- [3] Fung, Y. C. (1993). *An introduction to the theory of aeroelasticity*. Dover Publications, Inc., 1st edition.
- [4] George Washington Bridge (2018). Port authority of new york and new jersey. [online] <http://www.panynj.gov/bridges-tunnels/gwb-facts-info.html>.
- [5] Gimsing, N. J. (2006). *The Storebælt Publications - East Bridge*. A/S Storebæltsforbindelsen, 2nd edition.
- [6] Grinderslev, C.; Lubek, M. (2017). *Investigations of non-linear aeroelasticity of the Great Belt Bridge using CFD*. Aarhus: Aarhus University, 1st edition.
- [7] Krenk, S. (2001). *Mechanics and Analysis of Beams, Columns and Cables*. Springer-Verlag, 2nd edition.
- [8] Larsen, A. (1993). Aerodynamic aspects of the final design of the 1624m suspension bridge across the great belt. *Journal of Wind Engineering and Industrial Aerodynamics*.
- [9] Simiu, E.; Scanlan, R. (1986). *Wind effects on structures*. John Wiley and Sons, Inc., 2nd edition.
- [10] Tacoma Narrow Bridge (2018). Washington state department of transportation. [online] <http://www.wsdot.wa.gov/tnbhistory/machine/machine2.htm>.
- [11] Union Chain Bridge (2018). Friends of the union chain bridge. [online] <http://www.unionbridgefriends.com>.
- [12] Versteeg, H.; Malalasekera, W. (2007). *An introduction to Computational Fluid Dynamics - The Finite Volume Method*. Glasgow: Pearson Education Limited, 2nd edition.



APPENDIX

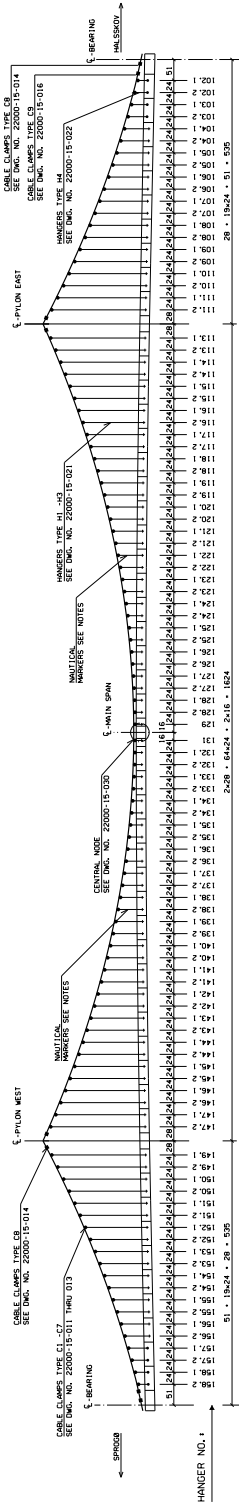


# PROJECT DRAWINGS FROM STOREBÆLT BRIDGE





ARRANGEMENT OF HANGERS AND CABLE CLAMPS  
(NOT TO SCALE)



**NOTES:**  
 ALL DIMENSIONS ARE IN METRES UNLESS OTHERWISE INDICATED.  
 CHARACTERISTIC DIMENSIONS ALONG BRIDGE REFER TO LEVEL 5.0.  
 BREAKING LOAD: 1700 kN/m<sup>2</sup> HANGER + 2 NO. PARALLEL WIRE STRANDS LENGTH, 100%  
 AS DEFINED ON DWGS. 22000-15-002, 020 & 022 CORRESPONDING TO THE HANGER TYPE.  
 A REFERENCE DIMENSION OF 127.0 IS USED FOR THE HANGER LENGTH.  
 DEAD LOAD AS DEFINED IN REF. 2.1.1. UNIFORM LEVEL OF HANGER. THE LOAD CORRESPONDS TO 2 STRANDS.  
 AVIATION HANGERS: BOLT HOLES FOR HANGERS TO BE PROVIDED AT BOTH SIDES OF CABLE CLAMPS AND CENTRAL NODES.  
 NAUTICAL HANGERS: TO BE INSTALLED AT HANGERS NO. 122.1 (NORTH SIDE ONLY) AND HANGER NO. 128.2 (SOUTH SIDE ONLY).  
 22000-15-002 HANGERS AND CABLE CLAMPS. GEOMETRY 22000-15-018 HANGERS AND CABLE CLAMPS. GEOMETRY 22000-15-021 HANGERS TYPE HH. DETAILS 22000-15-022 HANGERS TYPE HH. TOP BEARING DETAILS. 22000-15-024 HANGERS TYPE HH. BOTTOM BEARING DETAILS.  
 ORIGINAL DRAWING SCALE 1:1000  
 0 10 20 30 40 50 60 70 80 90 100

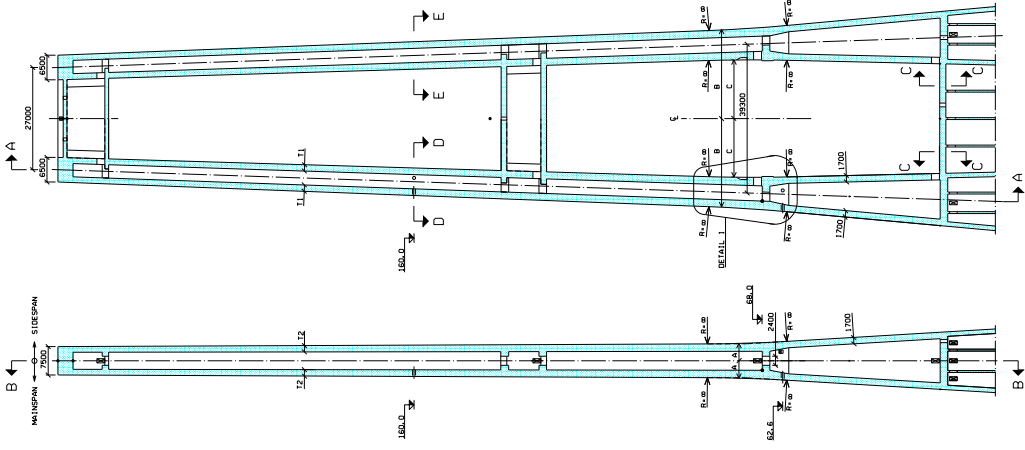
**DESIGN DATA, MAIN SPAN**

HANGER NO.	CROSS SECTION	SECTIONAL STEEL AREA (10 <sup>3</sup> CM <sup>2</sup> )	CHAR. HANGER FORCE (10 <sup>3</sup> kN)	NOMINAL HANGER BREAKING LENGTH (M)	SPACING OF CABLE CLAMPS (M)	CABLE CLAMP TYPE	AVIATION MARKERS
131.1	C52	2.4.3.2746.54	17.52	177.58	0.500	C5	X
131.2	C52	2.4.3.2746.54	17.52	177.58	0.500	C5	X
131.3	C52	2.4.3.2746.54	17.52	177.58	0.500	C5	X
131.4	C52	2.4.3.2746.54	17.52	177.58	0.500	C5	X
131.5	C52	2.4.3.2746.54	17.52	177.58	0.500	C5	X
131.6	C52	2.4.3.2746.54	17.52	177.58	0.500	C5	X
131.7	C52	2.4.3.2746.54	17.52	177.58	0.500	C5	X
131.8	C52	2.4.3.2746.54	17.52	177.58	0.500	C5	X
131.9	C52	2.4.3.2746.54	17.52	177.58	0.500	C5	X
132.0	C52	2.4.3.2746.54	17.52	177.58	0.500	C5	X
132.1	C52	2.4.3.2746.54	17.52	177.58	0.500	C5	X
132.2	C52	2.4.3.2746.54	17.52	177.58	0.500	C5	X
132.3	C52	2.4.3.2746.54	17.52	177.58	0.500	C5	X
132.4	C52	2.4.3.2746.54	17.52	177.58	0.500	C5	X
132.5	C52	2.4.3.2746.54	17.52	177.58	0.500	C5	X
132.6	C52	2.4.3.2746.54	17.52	177.58	0.500	C5	X
132.7	C52	2.4.3.2746.54	17.52	177.58	0.500	C5	X
132.8	C52	2.4.3.2746.54	17.52	177.58	0.500	C5	X
132.9	C52	2.4.3.2746.54	17.52	177.58	0.500	C5	X
133.0	C52	2.4.3.2746.54	17.52	177.58	0.500	C5	X
133.1	C52	2.4.3.2746.54	17.52	177.58	0.500	C5	X
133.2	C52	2.4.3.2746.54	17.52	177.58	0.500	C5	X
133.3	C52	2.4.3.2746.54	17.52	177.58	0.500	C5	X
133.4	C52	2.4.3.2746.54	17.52	177.58	0.500	C5	X
133.5	C52	2.4.3.2746.54	17.52	177.58	0.500	C5	X
133.6	C52	2.4.3.2746.54	17.52	177.58	0.500	C5	X
133.7	C52	2.4.3.2746.54	17.52	177.58	0.500	C5	X
133.8	C52	2.4.3.2746.54	17.52	177.58	0.500	C5	X
133.9	C52	2.4.3.2746.54	17.52	177.58	0.500	C5	X
134.0	C52	2.4.3.2746.54	17.52	177.58	0.500	C5	X
134.1	C52	2.4.3.2746.54	17.52	177.58	0.500	C5	X
134.2	C52	2.4.3.2746.54	17.52	177.58	0.500	C5	X
134.3	C52	2.4.3.2746.54	17.52	177.58	0.500	C5	X
134.4	C52	2.4.3.2746.54	17.52	177.58	0.500	C5	X
134.5	C52	2.4.3.2746.54	17.52	177.58	0.500	C5	X
134.6	C52	2.4.3.2746.54	17.52	177.58	0.500	C5	X
134.7	C52	2.4.3.2746.54	17.52	177.58	0.500	C5	X
134.8	C52	2.4.3.2746.54	17.52	177.58	0.500	C5	X
134.9	C52	2.4.3.2746.54	17.52	177.58	0.500	C5	X
135.0	C52	2.4.3.2746.54	17.52	177.58	0.500	C5	X
135.1	C52	2.4.3.2746.54	17.52	177.58	0.500	C5	X
135.2	C52	2.4.3.2746.54	17.52	177.58	0.500	C5	X
135.3	C52	2.4.3.2746.54	17.52	177.58	0.500	C5	X
135.4	C52	2.4.3.2746.54	17.52	177.58	0.500	C5	X
135.5	C52	2.4.3.2746.54	17.52	177.58	0.500	C5	X
135.6	C52	2.4.3.2746.54	17.52	177.58	0.500	C5	X
135.7	C52	2.4.3.2746.54	17.52	177.58	0.500	C5	X
135.8	C52	2.4.3.2746.54	17.52	177.58	0.500	C5	X
135.9	C52	2.4.3.2746.54	17.52	177.58	0.500	C5	X
136.0	C52	2.4.3.2746.54	17.52	177.58	0.500	C5	X
136.1	C52	2.4.3.2746.54	17.52	177.58	0.500	C5	X
136.2	C52	2.4.3.2746.54	17.52	177.58	0.500	C5	X
136.3	C52	2.4.3.2746.54	17.52	177.58	0.500	C5	X
136.4	C52	2.4.3.2746.54	17.52	177.58	0.500	C5	X
136.5	C52	2.4.3.2746.54	17.52	177.58	0.500	C5	X
136.6	C52	2.4.3.2746.54	17.52	177.58	0.500	C5	X
136.7	C52	2.4.3.2746.54	17.52	177.58	0.500	C5	X
136.8	C52	2.4.3.2746.54	17.52	177.58	0.500	C5	X
136.9	C52	2.4.3.2746.54	17.52	177.58	0.500	C5	X
137.0	C52	2.4.3.2746.54	17.52	177.58	0.500	C5	X
137.1	C52	2.4.3.2746.54	17.52	177.58	0.500	C5	X
137.2	C52	2.4.3.2746.54	17.52	177.58	0.500	C5	X
137.3	C52	2.4.3.2746.54	17.52	177.58	0.500	C5	X
137.4	C52	2.4.3.2746.54	17.52	177.58	0.500	C5	X
137.5	C52	2.4.3.2746.54	17.52	177.58	0.500	C5	X
137.6	C52	2.4.3.2746.54	17.52	177.58	0.500	C5	X
137.7	C52	2.4.3.2746.54	17.52	177.58	0.500	C5	X
137.8	C52	2.4.3.2746.54	17.52	177.58	0.500	C5	X
137.9	C52	2.4.3.2746.54	17.52	177.58	0.500	C5	X
138.0	C52	2.4.3.2746.54	17.52	177.58	0.500	C5	X
138.1	C52	2.4.3.2746.54	17.52	177.58	0.500	C5	X
138.2	C52	2.4.3.2746.54	17.52	177.58	0.500	C5	X
138.3	C52	2.4.3.2746.54	17.52	177.58	0.500	C5	X
138.4	C52	2.4.3.2746.54	17.52	177.58	0.500	C5	X
138.5	C52	2.4.3.2746.54	17.52	177.58	0.500	C5	X
138.6	C52	2.4.3.2746.54	17.52	177.58	0.500	C5	X
138.7	C52	2.4.3.2746.54	17.52	177.58	0.500	C5	X
138.8	C52	2.4.3.2746.54	17.52	177.58	0.500	C5	X
138.9	C52	2.4.3.2746.54	17.52	177.58	0.500	C5	X
139.0	C52	2.4.3.2746.54	17.52	177.58	0.500	C5	X
139.1	C52	2.4.3.2746.54	17.52	177.58	0.500	C5	X
139.2	C52	2.4.3.2746.54	17.52	177.58	0.500	C5	X
139.3	C52	2.4.3.2746.54	17.52	177.58	0.500	C5	X
139.4	C52	2.4.3.2746.54	17.52	177.58	0.500	C5	X
139.5	C52	2.4.3.2746.54	17.52	177.58	0.500	C5	X
139.6	C52	2.4.3.2746.54	17.52	177.58	0.500	C5	X
139.7	C52	2.4.3.2746.54	17.52	177.58	0.500	C5	X
139.8	C52	2.4.3.2746.54	17.52	177.58	0.500	C5	X
139.9	C52	2.4.3.2746.54	17.52	177.58	0.500	C5	X
140.0	C52	2.4.3.2746.54	17.52	177.58	0.500	C5	X

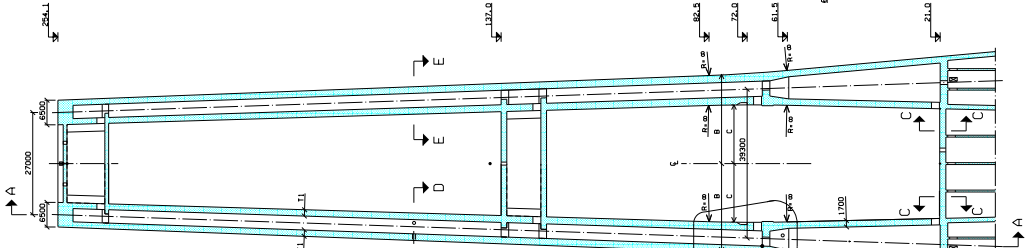
**DESIGN DATA, SIDE SPAN EAST**

HANGER NO.	CROSS SECTION	SECTIONAL STEEL AREA (10 <sup>3</sup> CM <sup>2</sup> )	CHAR. HANGER FORCE (10 <sup>3</sup> kN)	NOMINAL HANGER BREAKING LENGTH (M)	SPACING OF CABLE CLAMPS (M)	CABLE CLAMP TYPE	AVIATION MARKERS
100.1	C52	2.4.3.2746.54	10.37	13.700	0.600	C7	X
100.2	C52	2.4.3.2746.54	10.37	13.700	0.600	C7	X
100.3	C52	2.4.3.2746.54	10.37	13.700	0.600	C7	X
100.4	C52	2.4.3.2746.54	10.37	13.700	0.600	C7	X
100.5	C52	2.4.3.2746.54	10.37	13.700	0.600	C7	X
100.6	C52	2.4.3.2746.54	10.37	13.700	0.600	C7	X
100.7	C52	2.4.3.2746.54	10.37	13.700	0.600	C7	X
100.8	C52	2.4.3.2746.54	10.37	13.700	0.600	C7	X
100.9	C52	2.4.3.2746.54	10.37	13.700	0.600	C7	X
101.0	C52	2.4.3.2746.54	10.37	13.700	0.600	C7	X
101.1	C52	2.4.3.2746.54	10.37	13.700	0.600	C7	X
101.2	C52	2.4.3.2746.54	10.37	13.700	0.600	C7	X
101.3	C52	2.4.3.2746.54	10.37	13.700	0.600	C7	X
101.4	C52	2.4.3.2746.54	10.37	13.700	0.600	C7	X
101.5	C52	2.4.3.2746.54	10.37	13.700	0.600	C7	X
101.6	C52	2.4.3.2746.54	10.37	13.700	0.600	C7	X
101.7	C52	2.4.3.2746.54	10.37	13.700	0.600	C7	X
101.8	C52	2.4.3.2746.54	10.37	13.700	0.600	C7	X
101.9	C52	2.4.3.2746.54	10.37	13.700	0.600	C7	X
102.0	C52	2.4.3.2746.54	10.37	13.700	0.600	C7	X
102.1	C52	2.4.3.2746.54	10.37	13.700	0.600	C7	X
102.2	C52	2.4.3.2746.54	10.37	13.700	0.600	C7	X
102.3	C52	2.4.3.2746.54	10.37	13.700	0.600	C7	X
102.4	C52	2.4.3.2746.54	10.37	13.700	0.600	C7	X
102.5	C52	2.4.3.2746.54	10.37	13.700	0.600	C7	X
102.6	C52	2.4.3.2746.54	10.37	13.700	0.600	C7	X
102.7	C52	2.4.3.2746.54	10.37	13.700	0.600	C7	X
102.8	C52	2.4.3.2746.54	10.37	13.700	0.600	C7	X
102.9	C52	2.4.3.2746.54	10.37	13.700	0.600	C7	X
103.0	C52	2.4.3.2746.54	10.37	13.700	0.600	C7	X
103.1	C52	2.4.3.2746.54	10.37	13.700	0.600	C7	X
103.2	C52	2.4.3.2746.54	10.37	13.700	0.600	C7	X
103.3	C52	2.4.3.2746.54	10.37	13.700	0.600	C7	X
103.4	C52	2.4.3.2746.54	10.37	13.700	0.600	C7	X
103.5	C52	2.4.3.2746.54	10.37	13.700	0.600	C7	X
103.6	C52	2.4.3.2746.54	10.37	13.700	0.600	C7	X
103.7	C52	2.4.3.2746.54	10.37	13.700	0.600	C7	X
103.8	C52	2.4.3.2746.54	10.37	13.700	0.600	C7	X
103.9	C52	2.4.3.2746.54	10.37	13.700	0.600	C7	X
104.0	C52	2.4.3.2746.54	10.37	13.700	0.600	C7	X
104.1	C52	2.4.3.2746.54	10.37	13.700	0.600	C7	X
104.2	C52	2.4.3.2746.54	10.37	13.700	0.600	C7	X
104.3	C52	2.4.3.2746.54	10.37	13.700	0.600	C7	X
104.4	C52	2.4.3.2746.54	10.37	13.700	0.600	C7	X
104.5	C52	2.4.3.2746.54	10.37	13.700	0.600	C7	X
104.6	C52	2.4.3.2746.54	10.37	13.700	0.600	C7	X
104.7	C52	2.4.3.2746.54	10.37	13.700			

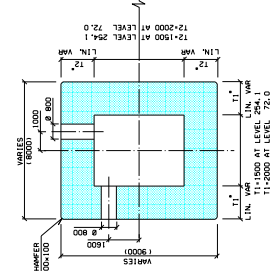
SECTION A-A, 1:500



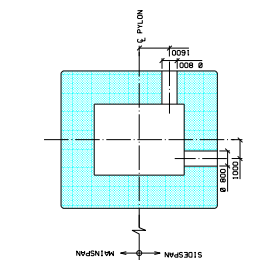
SECTION B-B, 1:500



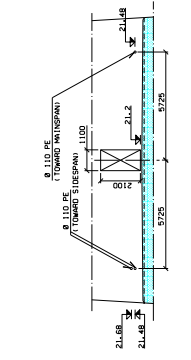
SECTION D-D, 1:100



SECTION E-E, 1:100



SECTION C-C, 1:100



SETTING-OUT TABLE

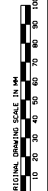
LEVEL	CURVE A	CURVE B	CURVE C
(M)	(M)	(M)	(M)
62.5	4497	2352	1039
63.0	4502	2357	1044
63.5	4507	2362	1049
64.0	4512	2367	1054
64.5	4517	2372	1059
65.0	4522	2377	1064
65.5	4527	2382	1069
66.0	4532	2387	1074
66.5	4537	2392	1079
67.0	4542	2397	1084
67.5	4547	2402	1089
68.0	4552	2407	1094
68.5	4557	2412	1099
69.0	4562	2417	1104
69.5	4567	2422	1109
70.0	4572	2427	1114
70.5	4577	2432	1119
71.0	4582	2437	1124
71.5	4587	2442	1129
72.0	4592	2447	1134
72.5	4597	2452	1139
73.0	4602	2457	1144
73.5	4607	2462	1149
74.0	4612	2467	1154
74.5	4617	2472	1159
75.0	4622	2477	1164
75.5	4627	2482	1169
76.0	4632	2487	1174
76.5	4637	2492	1179
77.0	4642	2497	1184
77.5	4647	2502	1189
78.0	4652	2507	1194
78.5	4657	2512	1199
79.0	4662	2517	1204
79.5	4667	2522	1209
80.0	4672	2527	1214
80.5	4677	2532	1219
81.0	4682	2537	1224
81.5	4687	2542	1229
82.0	4692	2547	1234
82.5	4697	2552	1239
83.0	4702	2557	1244
83.5	4707	2562	1249
84.0	4712	2567	1254
84.5	4717	2572	1259
85.0	4722	2577	1264
85.5	4727	2582	1269
86.0	4732	2587	1274
86.5	4737	2592	1279
87.0	4742	2597	1284
87.5	4747	2602	1289
88.0	4752	2607	1294
88.5	4757	2612	1299
89.0	4762	2617	1304
89.5	4767	2622	1309
90.0	4772	2627	1314
90.5	4777	2632	1319
91.0	4782	2637	1324
91.5	4787	2642	1329
92.0	4792	2647	1334
92.5	4797	2652	1339
93.0	4802	2657	1344
93.5	4807	2662	1349
94.0	4812	2667	1354
94.5	4817	2672	1359
95.0	4822	2677	1364
95.5	4827	2682	1369
96.0	4832	2687	1374
96.5	4837	2692	1379
97.0	4842	2697	1384
97.5	4847	2702	1389
98.0	4852	2707	1394
98.5	4857	2712	1399
99.0	4862	2717	1404
99.5	4867	2722	1409
100.0	4872	2727	1414

CURVE A: 0.0012102° ± 0.22022° ± 13.788 (M)  
 CURVE B: 0.0012102° ± 0.22022° ± 13.788 (M)  
 CURVE C: 0.0012102° ± 0.22022° ± 13.788 (M)

NOTES:  
 DIMENSIONS ARE IN MILLIMETRES UNLESS OTHERWISE INDICATED.  
 LEVELS ARE IN METRES DNN SYSTEM G1.  
 20-20 MM ON ALL EXTERNAL CORNERS OF CONCRETE UNLESS OTHERWISE INDICATED.  
 MATERIALS:  
 REINFORCEMENT: 20MM BARS  
 PIPES FOR PROTECTION OF PILES TO BE CAST-IN ALL LEVELS  
 MONITORING: REVISED

REFERENCES:  
 22000-23-012 PYLON FRAME, DIMENSIONS, LOWER CROSS BEAM  
 22000-23-014 PYLON FRAME, DIMENSIONS, UPPER CROSS BEAM

LEGEND:  
 REINFORCED CONCRETE, IN-SITU  
 CONSTRUCTION JOINT  
 REFERENCE SYSTEM FOR ELEVATIONS (LONGITUDINAL NML)  
 TANGENT POINT  
 SECTION POINT



ISSUED FOR CONSTRUCTION

NO.	DESCRIPTION	DATE	BY	CHECKED	STATUS
1	ISSUED FOR CONSTRUCTION	10/08/2022	MM	MM	ISSUED
2	ISSUED FOR CONSTRUCTION	10/08/2022	MM	MM	ISSUED

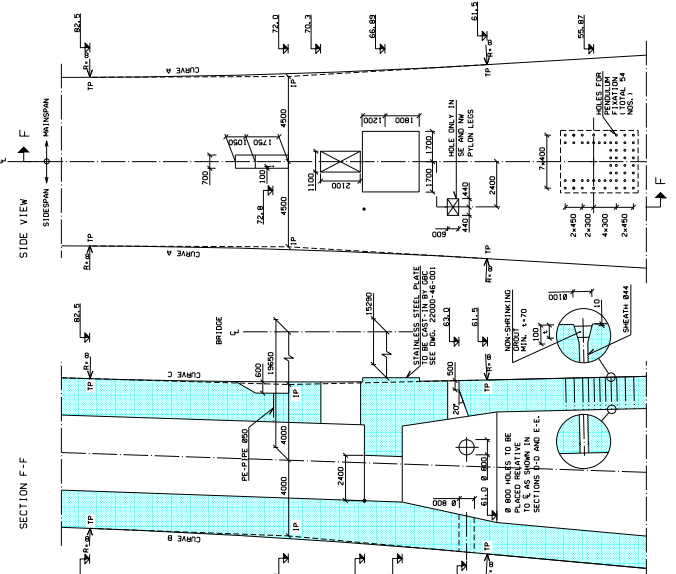
**Storeball**  
 Fixed Link across Storeball  
 East Bridge  
 Suspension Bridge  
 Detailed Design

Pylon Frame  
 Upper  
 Dimensions

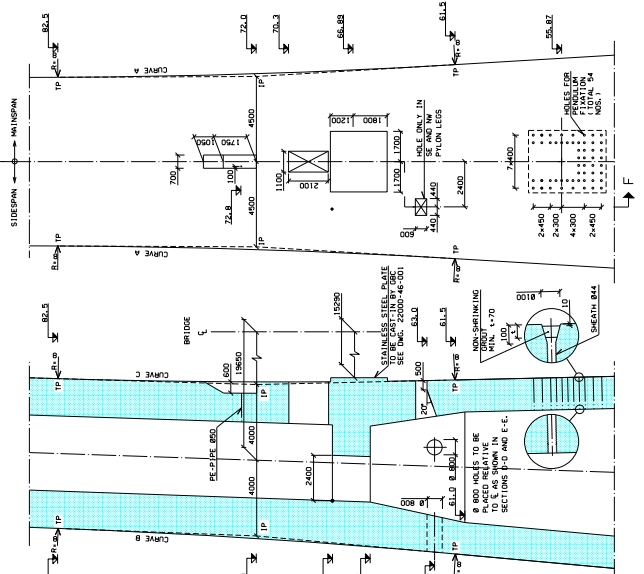
**CBR**  
 CONSULTANTS  
 CIVIL ENGINEERS & ARCHITECTS

PROJECT NO: 22000-23-010  
 SHEET NO: 2

DETAIL 1, 1:100



SECTION F-F



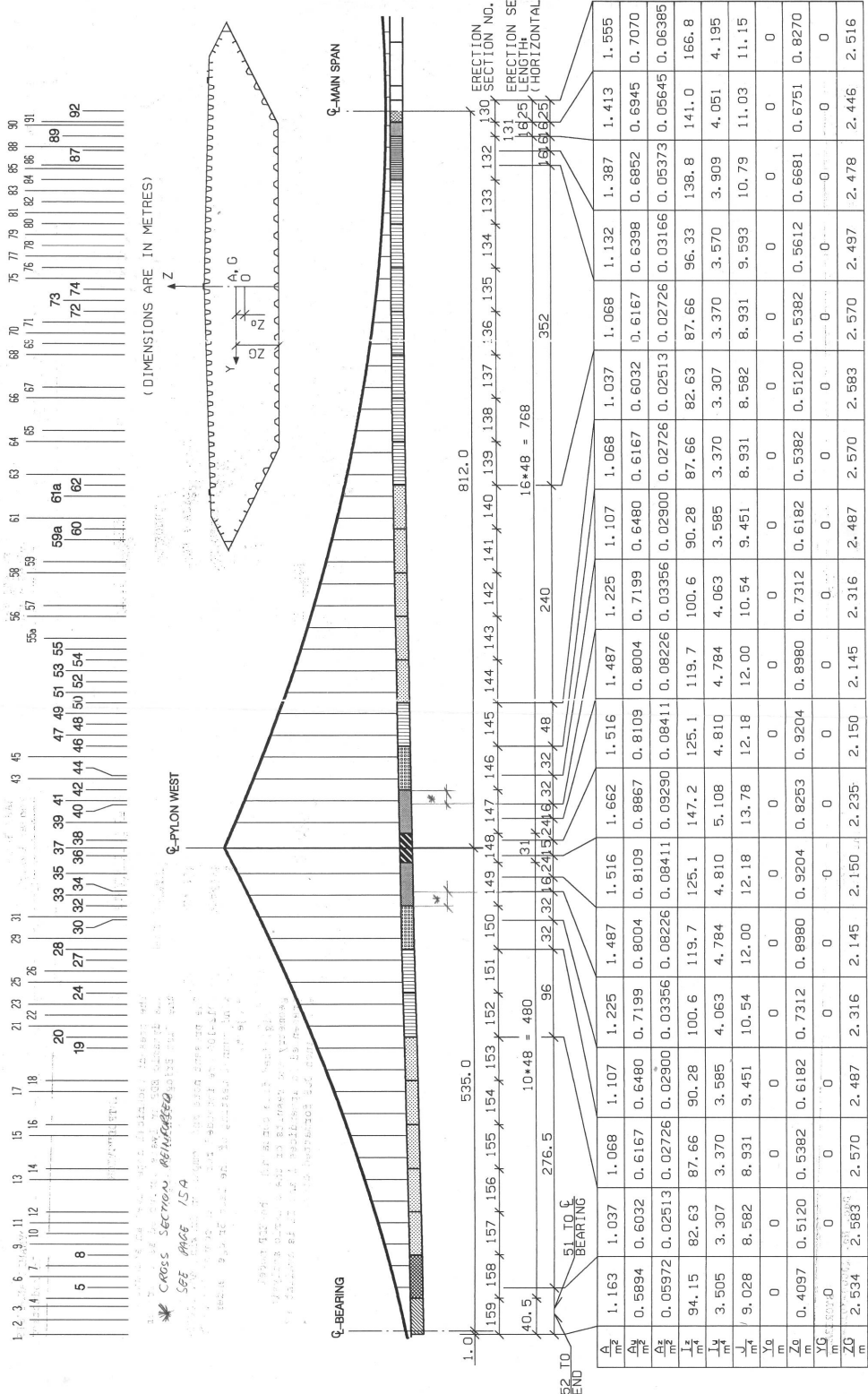


APPENDIX

B

## **CROSS SECTIONAL PARAMETERS OF GIRDER**

CBR o Joint Venture      Subject: EASI BRIDGE  
 Job No. 22000              SUSPENSION BRIDGE  
 Date: 30.09.2013          Designer: BRDR          Page 13.2.2-3  
 Date: 2/10/92              Check: *URR*



DATE: 2/10/92

BY: *URR*

SCALE: 1:50

PROJECT: EASI BRIDGE

SECTION: 13.2.2-3

DATE: 30.09.2013

BY: BRDR

CHECK: *URR*

SCALE: 1:50